1998

Seismic Velocity, Stratigraphy and Acoustic Study of the South China Sea

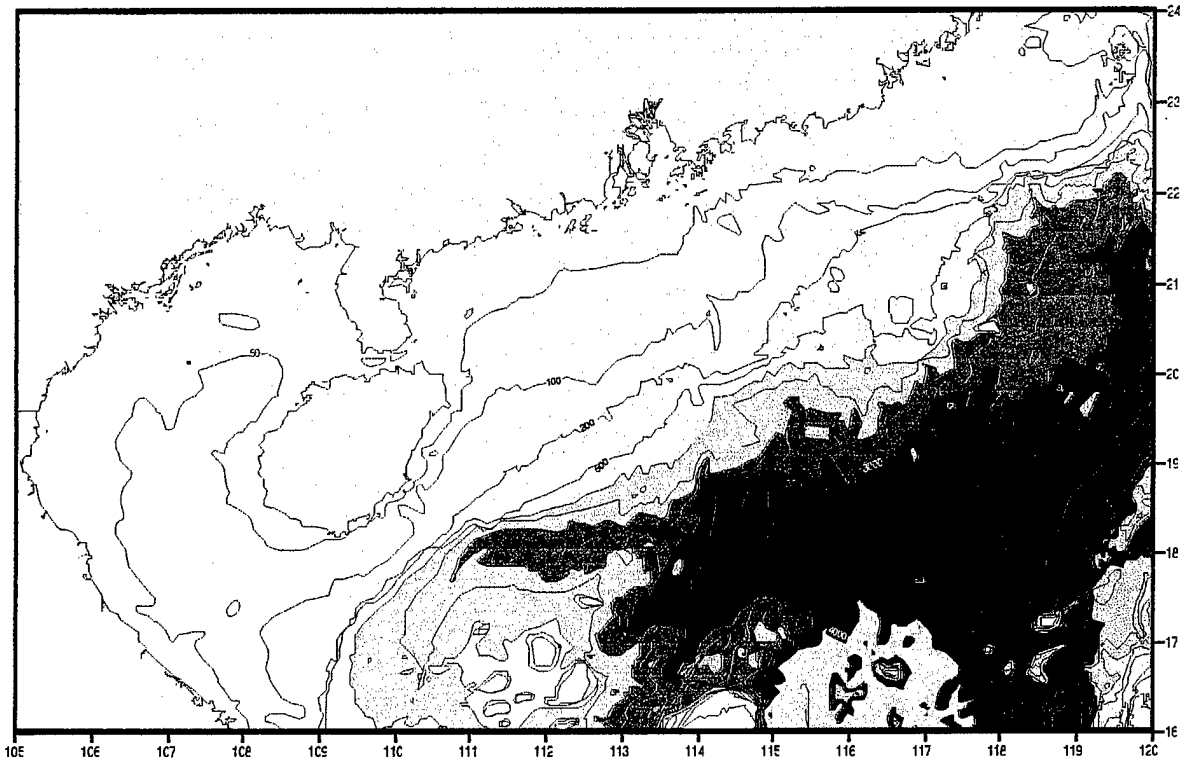

Peter D. Clift and Jian Lin

Department of Geology and Geophysics, Woods Hole Oceanographic Institution
Woods Hole, MA 02543, USA

WOODS HOLE OCEANOGRAPHIC INSTITUTION
1930

Award #: N00014-97-1-0902

WOODS HOLE OCEANOGRAPHIC INSTITUTION
Woods Hole, Massachusetts 02543
Phone: (508) 289-2227
FAX (508) 457-2187
Telex 951679

Department of Geology & Geophysics

October 13, 1998

Defense Technical Information Center
8725 John J. Kingman Road
STE 0944
Ft. Belvoir, VA 22060-6218

Dear Sir:

In compliance with the reporting requirements of ONR Grant No. N00014-97-1-0902 entitled "Seismic Velocity, Stratigraphy and Acoustic Study of the South China Sea", PIs Peter D. Clift and Jian Lin, enclosed are two copies for your files.

Sincerely yours,

Peter D. Clift

PDC:pf

Enclosure

REPORT DOCUMENTATION PAGE

OMB No. 0704-0188

1. AGENCY USE ONLY(*Leave Blank*)	2. REPORT DATE	3. REPORT TYPE AND DATES COVERED
	August 1998	Final

4. TITLE AND SUBTITLE
Seismic Velocity, Stratigraphy and Acoustic Study of the South China Sea

5. FUNDING NUMBERS
Award # N00014-97-1-0902

6. AUTHORS
Peter D. Clift and Jian Lin

7. PERFORMING ORGANIZATION NAME(S) AND ADDRESS(ES)
Department of Geology and Geophysics
Woods Hole Oceanographic Institution
Woods Hole, MA 02543

8. PERFORMING ORGANIZATION REPORT NUMBER

9. SPONSORING/MONITORING AGENCY NAMES(S) AND ADDRESS(ES)
Dr. Joseph H. Kravitz
Office of Naval Research, Ballston Tower 1
800 North Quincy Street, Arlington, VA 22217-5660

10. SPONSORING/MONITORING AGENCY REPORT NUMBER

11. SUPPLEMENTARY NOTES

12a. DISTRIBUTION/AVAILABILITY STATEMENT
Open report

12b. DISTRIBUTION CODE

13. ABSTRACT

A study was performed of the seismic velocity structure of the South China Shelf from the westernmost parts of the Beibu Gulf, adjacent to the Gulf of Tonkin, south of Hainan Island and offshore southern mainland China, as far east as 118°E. Stacking velocities from petroleum industry multichannel seismic surveys were compiled into a database from which the depth or two way travel time to any given velocity interval could be calculated. The data was filtered to remove major decreases in velocity with depth, as these normally reflected decreasing data quality below ~3 km. Data quality is typically good to 3 km, the approximate level of basement, and shows a good correlation with pre-existing seismic velocity data from sonobuoys.

Seismically the shelf sediments are usually flat bedded, with generally well defined reflective character. The slope does not appear to be strongly affected by slumping, although locally such disturbances are noted. The seismic data show that the sediment thicknesses are greatest offshore the Pearl River Mouth (up to ~5 km), where a large sedimentary basin is formed separated from the continental slope by an outer marginal basement high. Faulting in the basement is common and oriented coast-parallel. Later reactivation of these faults, sometimes results in their propagation to the seafloor.

14. SUBJECT TERMS
Multichannel seismic, velocity, South China, Beibu Gulf, Hainan

15. NUMBER OF PAGES
42

16. PRICE CODE

17. SECURITY CLASSIFICATION OF REPORT	18. SECURITY CLASSIFICATION OF THIS PAGE	19. SECURITY CLASSIFICATION OF ABSTRACT	20. LIMITATION OF ABSTRACT

Table of contents

1.0 Introduction 1

2.0 Data Coverage and Format 1
Map of South China Sea 2
Map of Data Available 3
Map of Data Compiled 5

2.1 Data Compilation 6
2.1.1 Multichannel Seismic Data 6
Map of Faults / Petroleum Wells 7
2.1.2 Well Data 8

3.0 Geological Setting and Other Related Studies 8
Example of Seismic Stratigraphy 9
Interpreted Across-Margin Profiles 10
Marine Magnetic Anomaly Map 12
3.0.1 Existing Seismic Data 13
Map of LDEO sonobuoys / Refraction Profile 14
3.0.2 Stratigraphic Framework 15
3.0.3 Subsidence Analysis 16
Subsidence Reconstructions 17

4.0 Seismic Velocity Structure 18
Maps of crust and mantle extension 19
Comparison of stacking MCS and ESP data 21

Velocity-Depth Maps 23

References 43

Appendix A 45

Seismic Velocity, Stratigraphy and Acoustic Study of the South China Sea

Peter D. Clift and Jian Lin

Department of Geology and Geophysics, Woods Hole Oceanographic Institution
Woods Hole, MA 02543

Award #: N00014-97-1-0902

1.0 Introduction

This report details the results of a twelve month project, spanning 1st June 1997 to 31st May 1998, to determine the velocity structure of the South China Shelf using released petroleum industry multichannel seismic reflection data. The project, undertaken for the Naval Oceanographic Office, was performed through a grant administered by the Office of Naval Research, Arlington, Virginia. The work was performed at the Woods Hole Oceanographic Institution by principle investigators Peter Clift (Assistant Scientist) and Jian Lin (Associate Scientist), with assistance from Research Assistant Lori Dolby, Staff Assistant May Reed and visiting students Eric Smail (Albion College) and Alissa Maxwell (Hamilton College). In essence the project involved the compilation of seismic velocity data from a series of multichannel seismic reflection surveys across the South China Shelf collected by British Petroleum (BP) and the Chinese National Oil Company (CNOOC), principally in 1979 and 1980. After abandoning their exploration efforts in the South China Sea these data were made available by BP/CNOOC to Clift and Lin for academic research purposes on a non-commercial basis. The velocity data was gathered into an electronic database for the purpose of examining the structure of the continental margin, with the long term scientific aims of understanding the nature of continental deformation during basin formation, as well as the history and controls on sedimentation along this passive margin.

2.0 Data Coverage and Format

The area considered in this project is shown in Figure 1. The data compiled under this project was all derived from paper multichannel seismic profiles, whose total coverage is shown on Figure 2. Electronic data was either not available or non-existent. The seismic data is of multichannel reflection type, usually 96 channel, most but not all of which was depth migrated during processing. Although BP were not willing to copy all of the data to us because of high associated

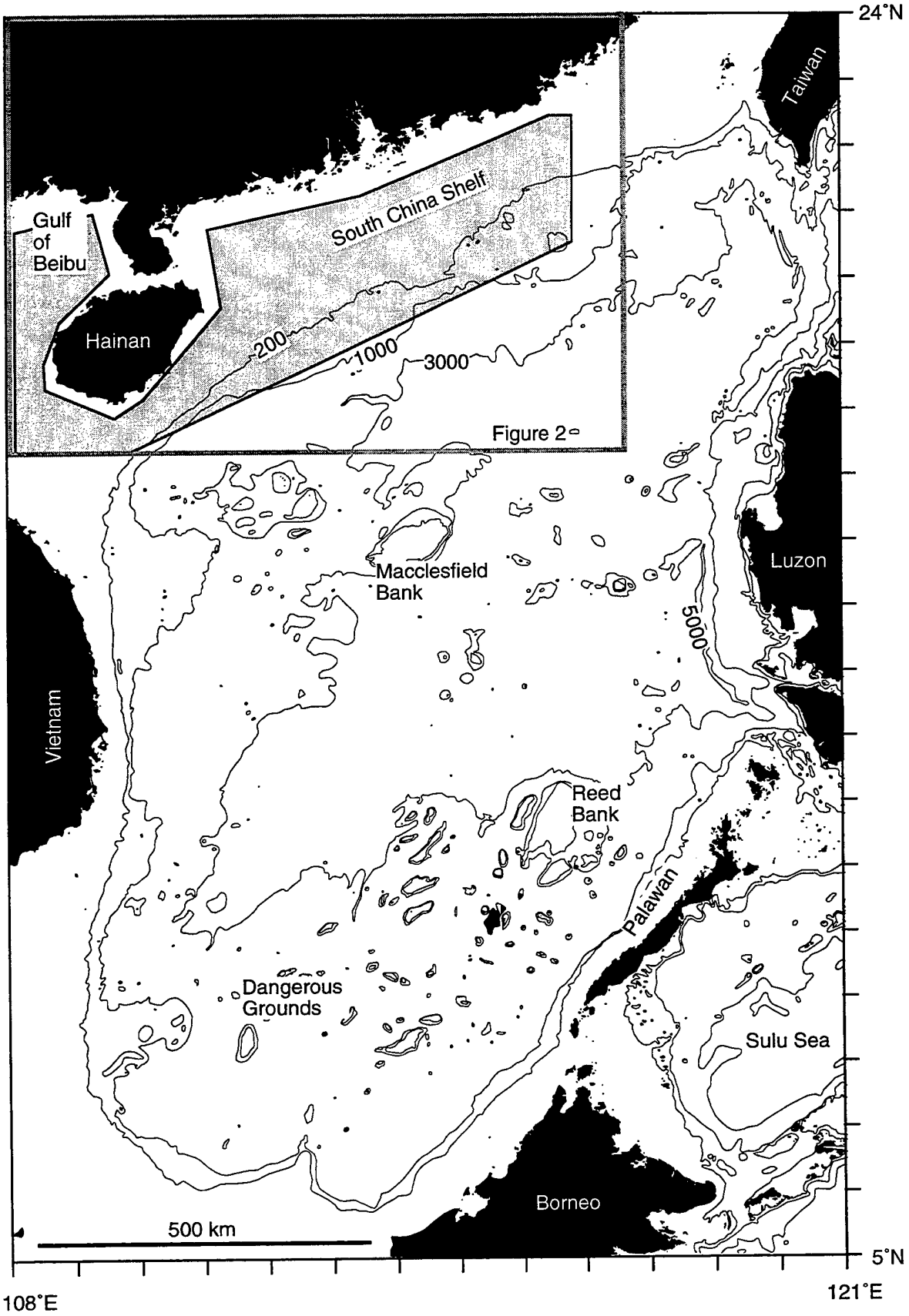

Figure 1. Bathymetric map of the South China Sea showing the survey area addressed by this project shaded in grey. Bathymetry in meters from GEBCO 1997 compilation.

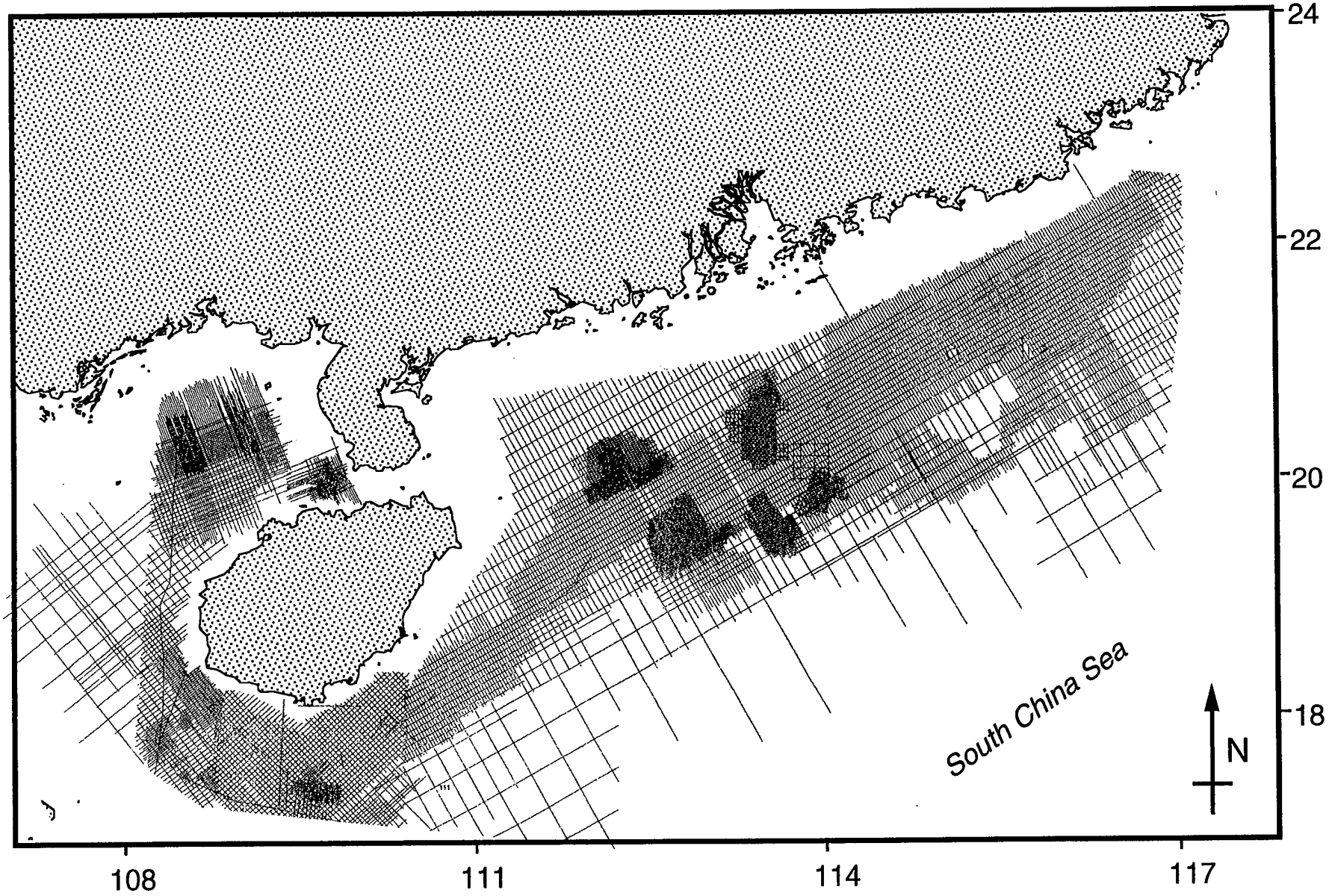

Figure 2. Map showing the coverage of multi-channel seismic lines released by BP and CNOOC for use by this project. Although not all the data was available for use at this stage, all the lines we requested were made available by BP and were incorporated into the database.

costs and the large manpower commitment entailed, all parts of the study area were covered. In practice BP's restriction was not significant because the sheer size of the entire data set would have made its processing within the time and manpower constraints of the project impossible. Access was typically sufficient to allow the 50 km resolution agreed in the original statement of work to be achieved. The velocity-depth structure of the margin was built up in three dimensions using a large number of one dimensional, vertical velocity profiles taken from the seismic profiles. On most of the seismic profiles the processing team had marked the two-way-travel time and root mean square (rms) velocities of seismic waves, that had been derived as the velocity data was stacked. In some instances the processors had also calculated interval (Dix) velocities, although we chose to ignore these and calculate our own values following the procedure set out by Dix (1955). This was done in order to ensure as much uniformity in the data as possible. We employed the equation

$$v_n = \left[\frac{V^2_{rms_n} t_n - V^2_{rms_{n-1}} t_{n-1}}{t_n - t_{n-1}} \right]^{1/2}$$

where $V_{rms_{n-1}}$, t_{n-1} and V_{rms_n}, t_n are the root-mean-square velocity and reflected ray travel times to the n-1th and nth reflectors respectively.

The spacing of the velocity control points depended strongly on which processing company handled the data. Despite the fact that all the data was jointly owned by a single consortium, BP/CNOOC, there were several companies involved in acquiring and processing the data. The calculated stacking velocities used to migrate the data were displayed at intervals along the top of the printed seismic reflection profile. It was these printed data that formed the input to our velocity model. Some companies had tightly spaced (< 1 km) velocity-time sections marked, while in other the spacing was wide (> 5 km), and in some cases sections were produced with no stacking velocities printed. In particular, a region of the shelf between 116°–117° E and 19°–21°N was principally surveyed by a Mobil/Chevron consortium that did not provide any stacking velocities and consequently our data coverage in this region is less good than anticipated (Fig. 3). The depth penetration of the seismic surveys was somewhat variable over the shelf. Data below 5 sec two-way-time (TWT) was usually not displayed, due to generally poor data quality at such depths in the shallow water of the shelf, as well as and lack of interest in the deep basement structure from the contracting companies. Data quality in the upper 2–3 km of the sedimentary cover was generally excellent, but background noise and other interferences became more significant below this point. In deeper water on the continental slope the lack of data below 5 sec TWT limited our ability to image the entire sediment cover overlying the basement.

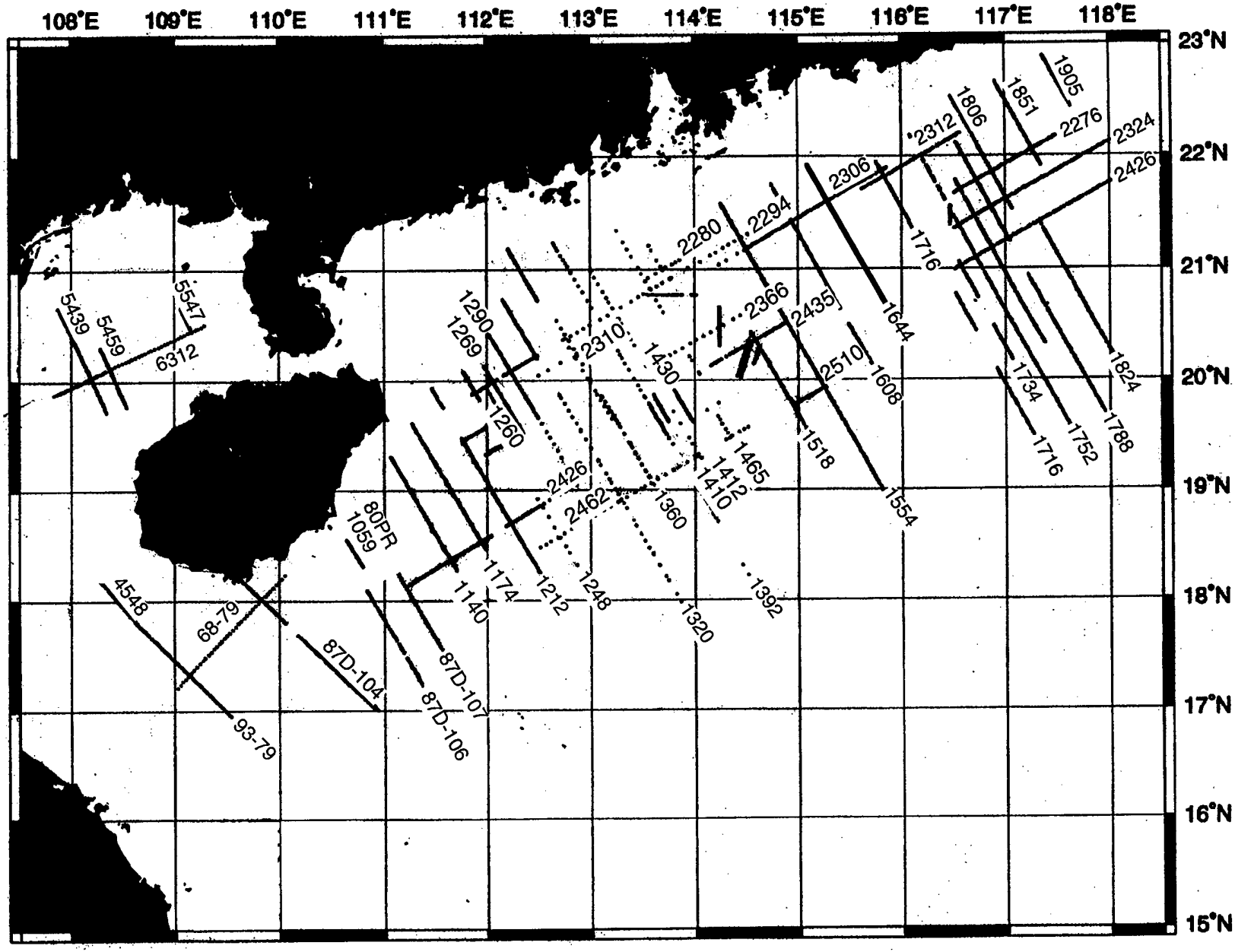

Figure 3. Map showing the distribution of data points at which the vertical seismic structure of the crust was determined from the seismic stacking velocities derived during the processing of the multichannel reflection data.

2.1 Data Compilation

2.1.1 Multichannel Seismic Data

The data compilation involved the manual retyping of the stacking velocities and two-way-travel times at each marked location (Fig. 3). The location of each control point was then marked on the available track line plots and the longitude/latitude of the point was determined by a digitizing procedure that entered the location data directly to the UNIX mainframe computer. The time-velocity data was originally entered into Microsoft *Excel* 5.0 on an Apple Macintosh and then transferred to the UNIX system after the calculation of the interval (Dix) velocities, using the formula shown above. Depths were also calculated from the rms velocity and the TWT. Once the given velocity structure had been acquired we chose to display the velocities at 500 m/s intervals. Since the sediment section at each of the control points was not neatly divided into 500 m/s packages, a routine was written for Maths Works *Matlab*, which calculated the depth/time to each of the chosen velocity steps from the velocity information provided. This was done by interpolating between the given data points and assuming a straight line progression between points, so that depths to different velocity breaks can be calculated. This process was able to standardize the input data, which was not uniform from company to company. In some sections the rms velocity was provided at regular TWT intervals down-section, while in other cases the rms velocity was provided where there was jump in velocity, i.e., at major reflectors. The electronic database thus provides at any given location, the time and depth to a series of velocity intervals, spaced at 500 m/s. The velocity provided corresponds to maximum compressional wave velocity.

The end product of the data compilation is a series of maps showing the time or depth to any set velocity interval starting at the seafloor. Those lines that were actually entered into the electronic database are shown in Figure 3. Maps provided with this report are shown in two modes, one with just the velocities around the immediate areas of the control points, i.e., the actual data, and another with the velocities extrapolated between the control points to cover the entire area of the shelf. These extrapolated maps are most reliable in the upper part of the section, where the reflection data support the approximation of a layer cake stratigraphy over much of the area. However, at depth faulting on a scale smaller that the distance between seismic profiles makes extension of the velocities contours a meaningless exercise. A more comprehensive survey of the entire database by BP Exploration, including interpretation of the reflection images, allowed them to identify the major fault lineaments and to define the lateral extent of the major syn-rift depocenters (Fig. 4). Cross checking of this map through the data provided to this project has confirmed the general validity of the map.

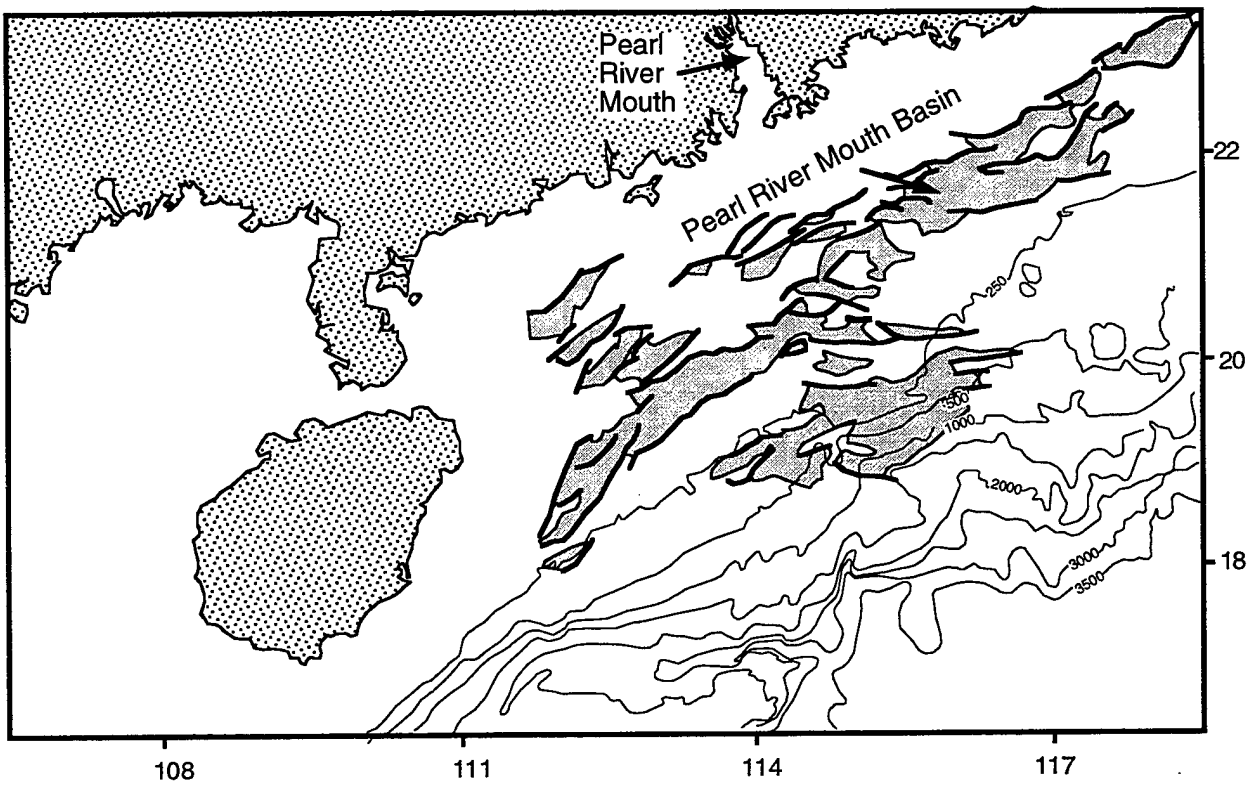

Figure 4. Location of the major fault lineaments and associated sedimentary basins on the South China Shelf compiled from BP/CNOOC mulitchannel seismic data.

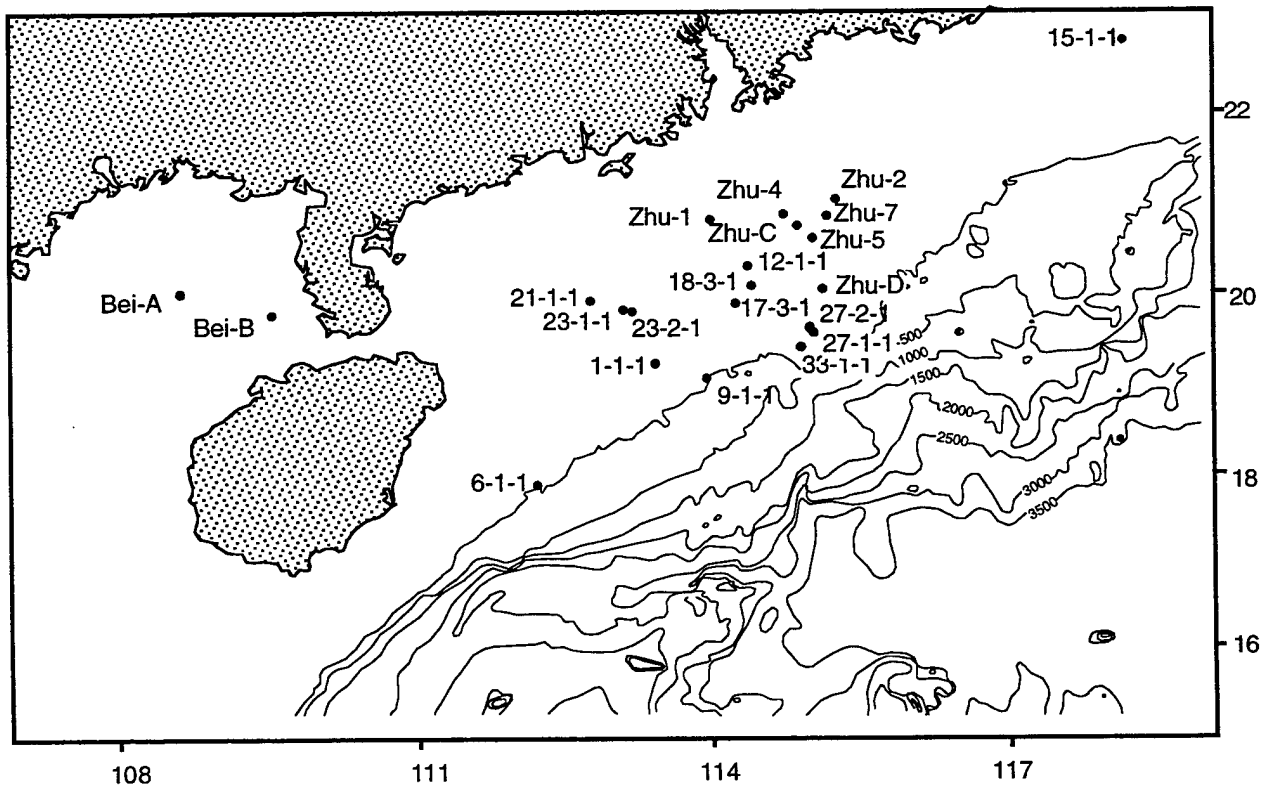

Figure 5. Location of petroleum exploration wells for which lithologic and biostratigraphic data were available for the completion of this project.

2.1.2 Well Data

The correlation of velocity to lithology was possible thanks to access to 22 well logs (Fig. 5). 15 of the wells penetrated to crystalline basement, with the remainder bottoming in syn-rift alluvial clastic sediments of Eocene–Oligocene age. Four of the wells, Bei-A, Bei-B, Zhu-5 and Zhu-7 are derived from the work of *Su et al.* [1989], at which the original well data was not available. Geophysical well logs were typically not available, so that it was not possible to cross-check the stacking velocities with in situ measurements of the sonic velocity. Nonetheless, the drilled sections were useful in demonstrating a good agreement between the predicted depth of the pre-rift crystalline basement at a velocity of > 4500 m/s and the occurrence of these velocities in the well cuttings. The wells also provide a good opportunity to assign biostratigraphic ages to the seismic reflectors. Figure 6 shows examples of two wells, Panyu 27-1-1 and Panyu 27-2-1 in the central part of the South China Shelf, on the rim of the Pearl River Mouth Basin, one of the largest depocenters encountered in the region. The reflection data show that Panyu 27-1-1 is located on the crest of a rotated fault block and consequently does not sample any of the oldest syn-rift sediments in the basin center. Since petroleum wells usually target the structural highs where hydrocarbon accumulations might be expected, this is a common short coming of the wells in this region. Panyu 27-2-1 is also located on the edge of the Pearl River Mouth Basin, but this is located on the downthrown, hanging wall block of a large fault and so penetrated some of the syn-rift strata. The analysis of microfossil assemblages within the sediments allows the depositional history of sediments on the margin to be reconstructed. Four example cross sections of the South China Margin are shown in Figure 7 in which one or more well ties were extrapolated over the shelf and on to the continental slope. In contrast to the sections derived from the stacking velocities the horizons identified on these sections are considered roughly isochronous. Interpretation of the profiles allows the overall geometry of the sedimentary fill and architecture of the faulting to be determined. While the top ~1 km of the shelf is marked by relatively flat lying sediment, disrupted by minor fault reactivation, the basement structure below this level is very rough, reflecting the extensional faulting of the original extensional deformation.

3.0 Geological Setting and Other Related Studies

The South China Sea was formed by oceanic spreading along a WSW-ENE axis during the Oligocene–Miocene [*Taylor and Hayes*, 1980; *Lu et al.*, 1987; *Briais et al.*, 1993], although extension in the area is believed to have started as early as the Late Cretaceous–Early Paleocene [*Schlüter et al.*, 1996]. Propagation of oceanic spreading towards the WSW resulted in a V-shaped area of oceanic crust bounded to the east by an east-dipping subduction zone, and to the west by

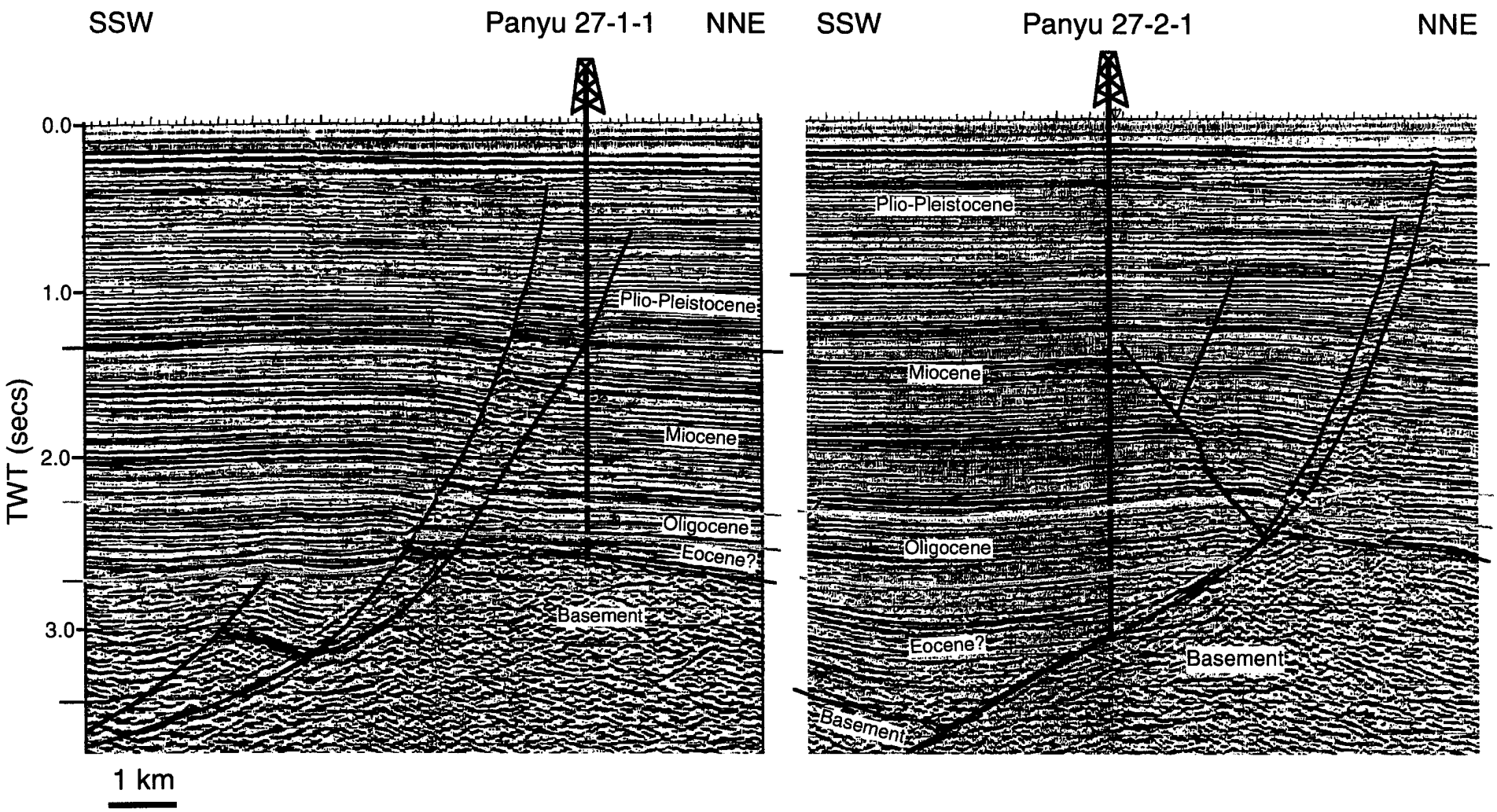

Figure 6. Interpreted multichannel seismic lines showing the location of well Panyu-27-1- on a hangingwall block that does not penetrate the syn-rift sequences and Panyu 27-2-1 which cuts the feather edge of the syn-rift. In the ccase of other South China lines the noise volumes on the lines are low, allowing easy recognition of prominent seismic horizons that can be dated through appropriate well ties.

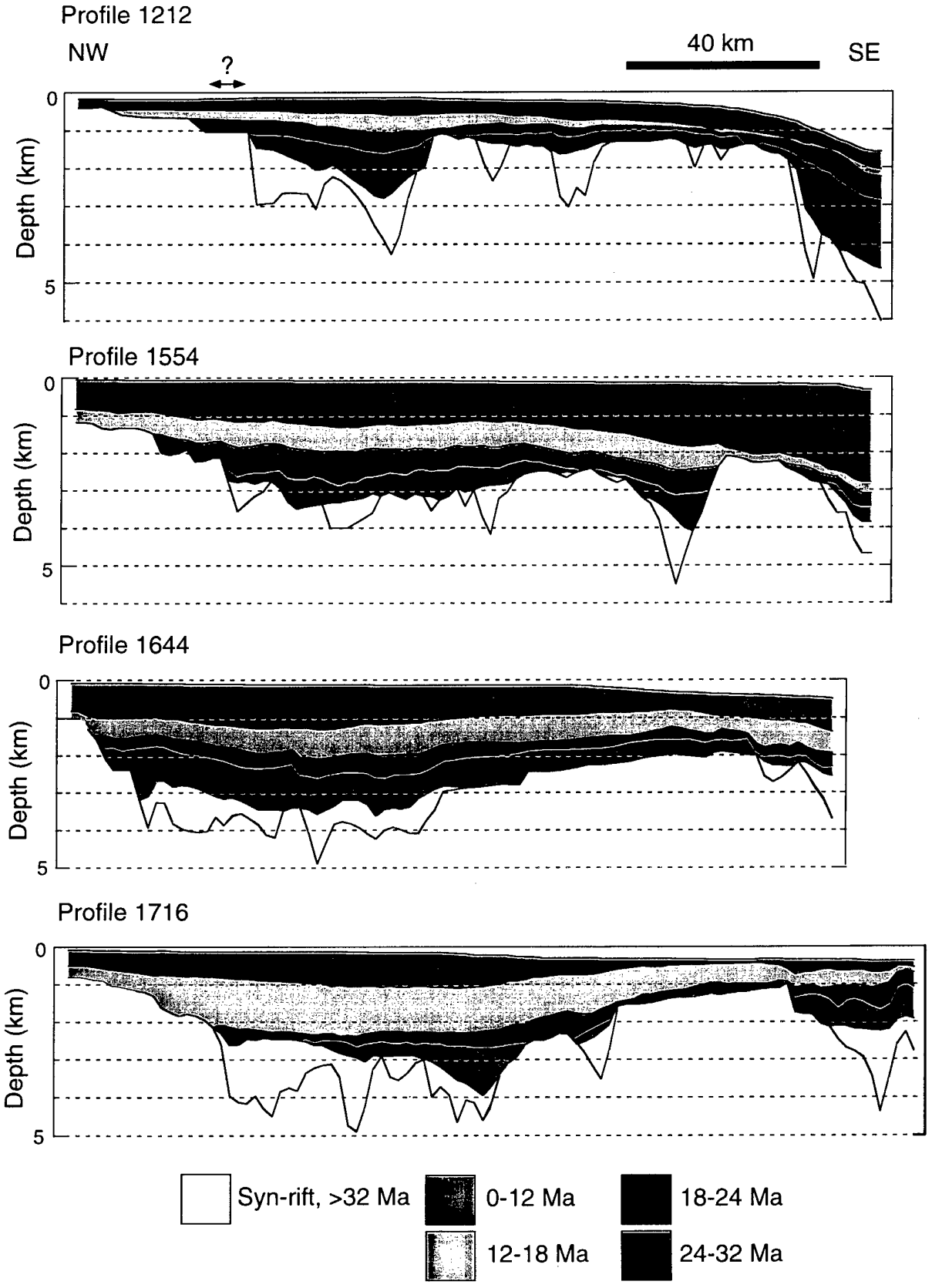

Figure 7. Interpreted cross sections of the South China Shelf and upper slope, showing outer structural high separating the Pearl River Mouth basin from the South China Slope. Age assignments are derived from ties with nearby wells. See Figure 3 for location.

the termination of the rift close to the southern end of Indo-China, a margin interpreted as having a transform, sheared character due to its steep gradient and association with the strike-slip Red River Fault at its northern end. Extension on the proto-South China Shelf prior to seafloor spreading resulted not only in increasing extension towards the oceanic crust and the generation of a series of tilted fault blocks under the slope adjacent to the continent-ocean transition, but also a series of sedimentary basins, separated from the main rift axis by blocks of less extended crust (Fig. 7). The Pearl River Mouth Basin is the largest such basin on the north side of the South China Sea and dominates the structure of the central shelf. Extension during continental break-up clearly did not simply increase across the continent-ocean transition, as shown by the presence of two large, relatively unextended crustal blocks, the Macclesfield and Reed Banks close to the continent-ocean transition (Fig. 1). Their generation is partially linked to complexities in the seafloor spreading history, as marine magnetic anomalies show that the original rift axis was positioned between Macclesfield Bank and the main South China Shelf and then jumped to a southerly position before propagating further WSW [Fig. 8; *Taylor and Hayes*, 1980; *Briais et al.*, 1993]. Interpretation of the magnetic anomalies places the start of seafloor spreading at ~30 Ma (Early Oligocene, Rupelian), finishing at ~16 Ma (Middle Miocene, Langhian).

Using reflection seismic and drilling data, *Schlüter et al.* [1996] suggested that extension along a north-dipping simple shear system was responsible for the formation of the marginal basins on the south side of the South China Sea, i.e., the Dangerous Grounds, Reed Bank and Palawan continental margin (Fig. 1). Subsequently this southern rift axis was abandoned in favor of the main northern rift axis. It is still unclear as to what the driving mechanisms for the regional extension are. Various workers [e.g., *Holloway,* 1982; *Taylor and Hayes*, 1983; *Liu et al.*, 1987] have suggested that extension was related to southward subduction under Borneo, with the southern margin (i.e., Dangerous Grounds, Reed Bank, North Palawan Block; Fig. 1) being displaced southward relative to mainland China and Indochina along a major N-S trending transform zone on the west side of the basin (i.e., the Vietnam margin). Some influence has also been attributed to northward subduction beneath the Philippines driving a backarc type of extension in the overriding plate [*Taylor and Hayes*, 1980].

In contrast, *Wheeler and White* [1997] noted that the correlation of extension factors derived from modeling of well data and crustal thickness measurements indicated that dynamically driven subsidence due to subduction is not a factor in driving basin formation in the South China Sea. They further replicated the results of an earlier study by *Su et al.* [1989] in estimating total crustal extension in the center of the Pearl River Mouth Basin of the South China Shelf at $\beta = 1.8$, and indicated that extension was a uniform, pure shear process that was completed by ~25 Ma (Late Oligocene, Chattian).

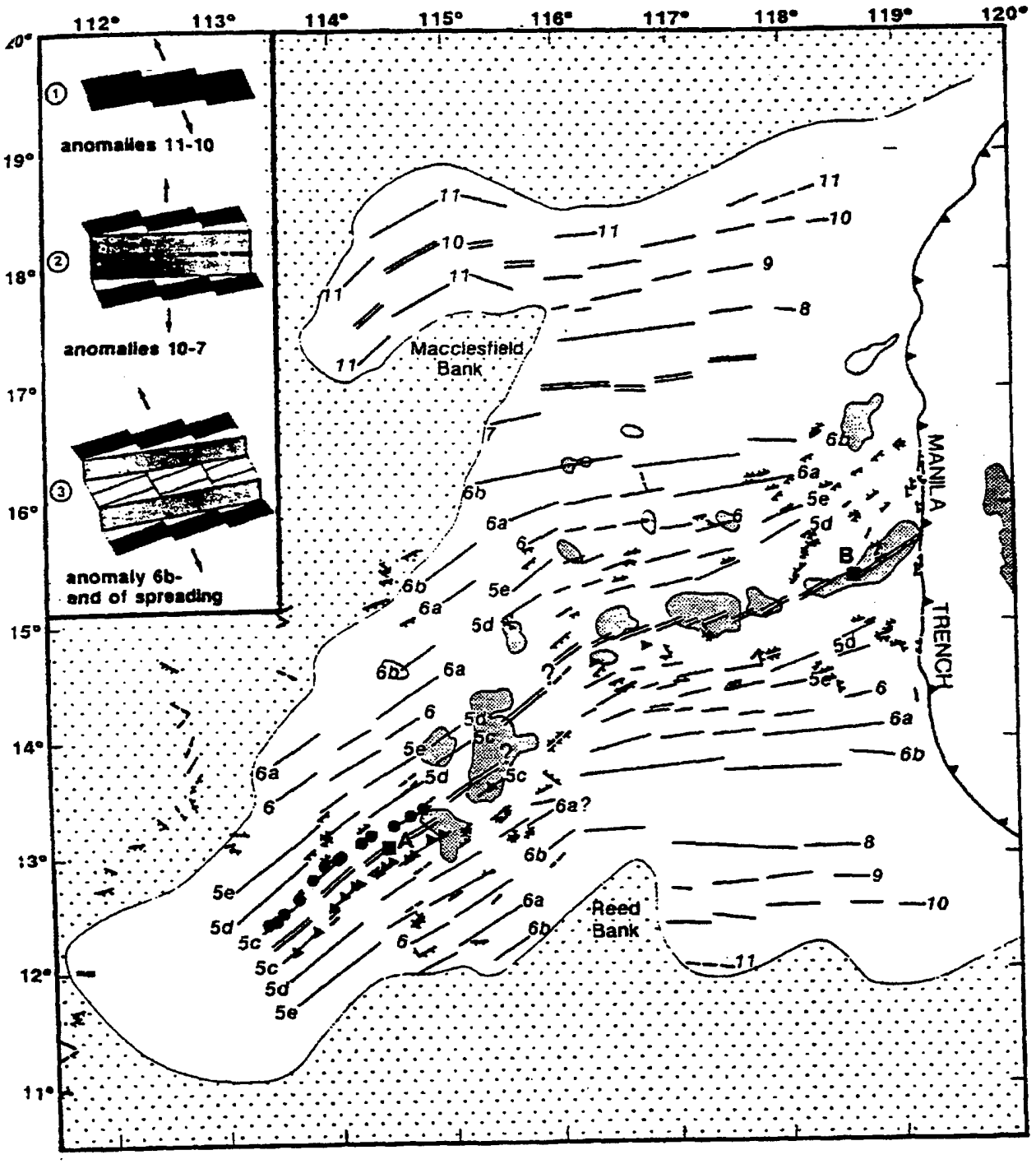

Figure 8. Magnetic lineations in South China Sea interpreted by *Briais et al.* [1993] showing the clear SW-directed propagation of the ridge and the ridge jump from north to south of the Macclesfield Bank between anomaly 10 and 9 times.

Alternative mechanisms for driving the extension in the South China Sea [e.g., *Tapponnier et al.*, 1982; *Peltzer and Tapponnier*, 1988] favor extension due to the southeastward motion of Indochina and Borneo relative to a fixed China. In this scenario differential motion is due to extrusion of Indochina following the indentation of India into Asia during the Early Tertiary. Specifically Indochina motion relative to mainland Asia is linked to the Red River Fault system, the northern extension of the Vietnamese transform margin. *Harrison et al.* [1996] used $^{39}Ar/^{40}Ar$ dating of metamorphic rocks from along the Red River shear system to show that this fault system initiated close to the time of South China Sea spreading, ~25 Ma along the fault in northern Vietnam, and that motion was of the same rate as spreading determined from magnetic anomalies. In contrast, *Burchfiel et al.* [1997] used combined radiometric, paleomagnetic and structural data to suggest that while extrusion of Indochina relative to Asia did occur synchronous with spreading in South China Sea, this was of insufficient magnitude to account for the total width of spread crust. Similarly, in a synthesis of SE Asian tectonics, *Packham* [1996] pointed out that not only did spreading in South China Sea stop after the end of motion on the Red River Fault (15.5 Ma compared to 17–19 Ma; *Leloup et al.*, 1993), but that due to a jump in the orientation of spreading axes in the basin at 24–26 Ma (between anomaly 7 and 6b) the southern margin subsequently moved obliquely away from Indochina, thus eliminating motion along the Red River Fault as a driving mechanism for extension after this time. The link between opening of the South China Sea is still controversial, although it seems unlikely that motion on the fault alone is responsible for extension.

3.0.1 Existing Seismic Data

The South China Margin has been surveyed by deep refraction seismic methods along three transects [Fig. 9; *Nissen et al.*, 1995a, b; *Hayes et al.*, 1995], providing an image of the whole crustal structure at a broad scale. This analysis showed overall thinning of the crust towards the continent-ocean transition along much of the margin, although in the east of the South China Shelf the lower crust (>15 km) appears to have higher velocity (> 7.0 km/s; Fig. 10) than that in the west. Such velocities are intriguing because elsewhere such values have been related to the presence of gabbro underplated to the base of the crust during break-up along volcanic margins [e.g., East US Coast, *Holbrook and Kelemen*, 1995; Hatton Bank, *White et al.*, 1987]. However, the lack of the seaward-dipping lavas that characterize volcanic margins [*Hinz*, 1981] means that South China cannot be considered a classic volcanic margin. The suggestion of underplating does, however, raise the possibility of this area being intermediate in terms of volcanism between the end member volcanic and non-volcanic [e.g., Iberia; *Boillot et al.*, 1995; *Sibuet et al.*, 1995; *Reston et al.*, 1995] examples described to date.

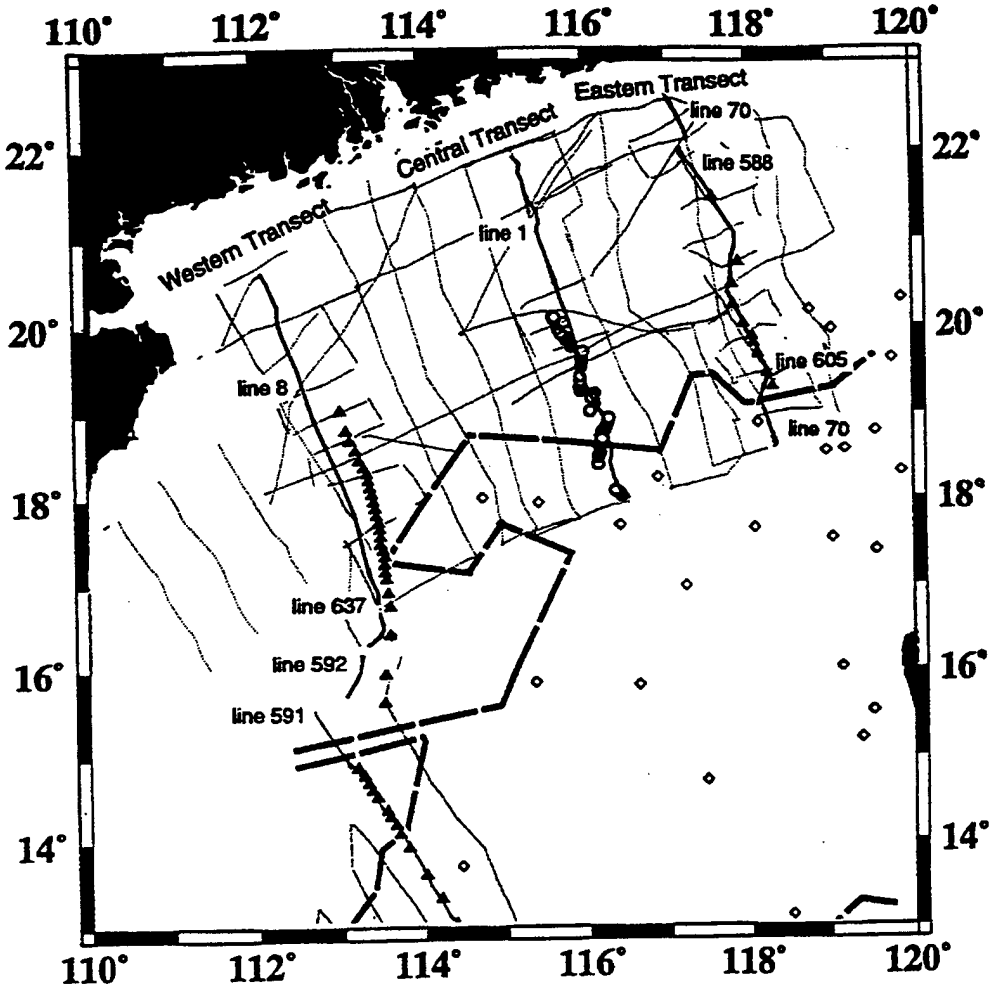

Figure 9. Map showing the location of the deep seismic lines and heatflow data collected by the Lamont-Doherty group [from *Nissen et al.*, 1995]. Solid triangles, diamonds and open circle show heatflow data collection stations. Dotted lines show the seismic lines available to this study. The heavy dashed line is the interpreted position of the continent-ocean transition.

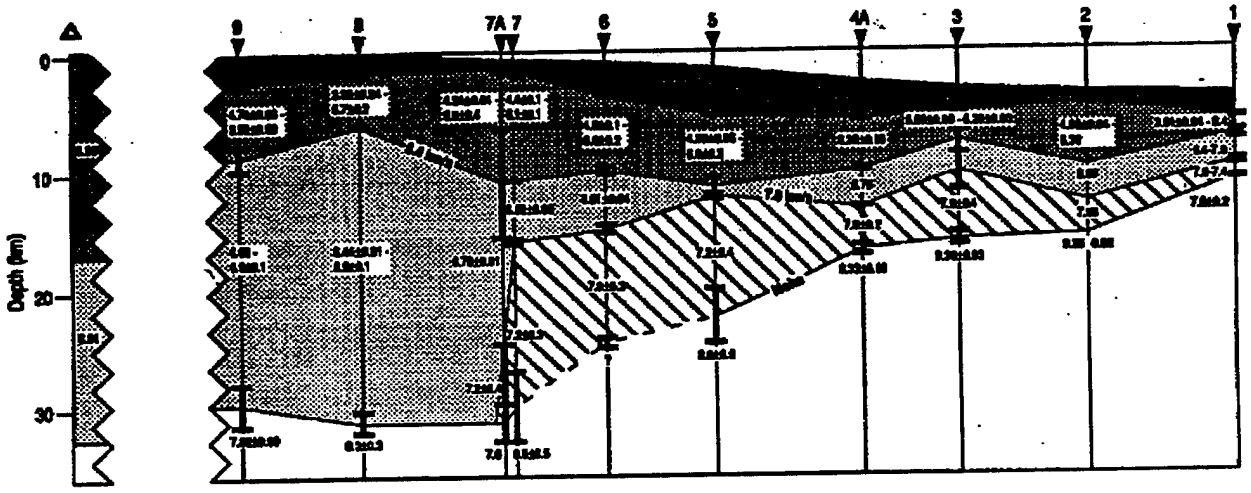

Figure 10. Depth section obtained from ESP interpretation across the South China margin showing the thinning of crust towards the COT and the high-velocity material at the base of the crust that may represent magmatic underplating, similar to those seen on rifted volcanic margin [after *Nissen et al.*, 1995].

Reflection seismic data from South China Sea have been sparse in the published literature. Short sections of industrial seismic reflection data have been published in support of reconstructed fault maps of the shelf [e.g., *Edwards*, 1992; *Zhiqiang et al.*, 1992]. However, the only large scale data previously available is in the form of three interpreted line drawings from the central Pearl River Mouth basin [*Su et al.*, 1989].

3.0.3 Stratigraphic Framework

However the extension is driven, what is clear is that the South China margin is linked to the propagation of an oceanic spreading center during the Late Oligocene, that separated two rifted continental areas, the South China margin and the conjugate Dangerous Grounds/Palawan margin (Fig. 1). The passive margin sediments that accumulated in the associated basins are best known from the Pearl River Mouth Basin, where they have been sampled by numerous petroleum exploration wells. The sediments are typically continental, alluvial at the base and show a deepening upward into shelf siliciclastics. Detailed biostratigraphic work, coupled with lithologic variation has allowed the subdivision of the section into nine separate formations [*Su et al.*, 1989]. Thin Maastrichtian sediments are present locally, succeeded by continental, alluvial Paleocene to Early Eocene siltstones and sandstones. From Early to Middle Eocene dark lacustrine shales were deposited, succeeded in turn by Early Oligocene coal-bearing swamp and littoral plain sediments. Following the major extensional episode of the Eocene–Oligocene, sedimentation became submarine, more neritic at first, then later bathyal further offshore. Much of the sediment deposited on the shelf today is derived from the Pearl River in the central area or from the Red River in the westernmost areas, west of Hainan, in the Gulf of Beibu and Song Hong Basin of the Gulf of Tonkin. These sediments are for the most part eroded from the eastern Himalayas, as well as the Ailao Shan of SW China. Dating of the sediments is well constrained following marine transgression in the Oligocene. Earlier ages, within the syn-rift deposits, are generally determined by palynological methods, which provide an Eocene–Oligocene determination. Consequently, the age and duration of the syn-rift episode is not tightly controlled, although the end of rifting can be limited to prior to ~32 Ma based on nannofossil determinations from post-rift sediment, which can be observed as being undisturbed by the main extensional event. When determining ages we follow the timescale of *Berggren et al.* [1995], using the nannofossil and foraminiferal zone determinations from well logs at each of the sites considered.

Table 1. Stratigraphic Division of the Pearl River Mouth Basin [after *Chen et al.*, 1987].

Age at base (Ma)	Epoch	Formation	Thickness (m)
1.8	Quaternary		200
5.3	Pliocene	Wanshan	100–450
12	Late Miocene	Yuehai	200–600
14	Mid Miocene	Hanjiang	500–1100
24	Early Miocene	Zhujiang	350–750
35	Late Oligocene	Zhuhai	500–1100
43.5	Eocene-Oligocene	Enping	1100–1600
54	Eocene	Wenchang	1000-2000
65	Paleocene	Shenhu	0–1000

3.03 Subsidence Analysis

The vertical motions of the South China Shelf through time can be reconstructed using the stratigraphies drilled in the exploration wells. In order to quantify these motions, we employed the one dimensional backstripping method by which the vertical motion of the basement at a given drill site can be tracked through time, by accounting for the loading effects of sediment and water, as well as fluctuations in the global eustatic sealevel [*Sclater and Christie*, 1980]. The input data for this analysis are lithology, age, and water depth of sedimentation, all of which can be derived from standard oil industry well logs. Stratigraphic age is determined using biostratigraphic data and is converted to a numerical age using the scheme of *Berggren et al.* [1995]. The physical parameters of each sediment type, in terms of density, porosity and compaction characteristics, are taken from *Sclater and Christie* [1980], based on measurements from the North Sea. The simple one dimensional method developed by *Sclater and Christie* [1980] assumes local isostatic compensation, a reasonable approximation where the lithosphere is weak or the applied load is wide and evenly distributed. Studies of extensional sedimentary basins such as the North Sea [e.g., *Barton and Wood*, 1984] have indicated that the lithosphere beneath sedimentary basins is very weak (effective elastic thickness <5 km) during the rifting and early postrift period. *Karner and Watts* [1982] showed that the rifted continental crust of the Coral Sea and Lord Howe Rise still only has an elastic thickness of 5 km, although rifting was complete at 60 Ma. It is thus likely that the crust of the South China Shelf may also be flexurally weak, because rifting there is even younger than the Coral Sea, i.e., ~32 Ma, a prediction supported by the gravity work of *Wheeler and White* [1997]. Knowledge of the structural position of the well is also important in the interpretation of the reconstruction, since compared to a perfectly plastic plate wells situated on the hanging wall will tend to show more synrift sedimentation than those on the footwall. Postrift thermal subsidence will tend to be the same for each location.

Estimates of paleo-water depth are often a source of error when attempting backstripping subsidence analysis. In this setting, however, most of the wells lie on the shelf, typically in around 100 m of water. Well logs show continental or shallow marine facies through the column since

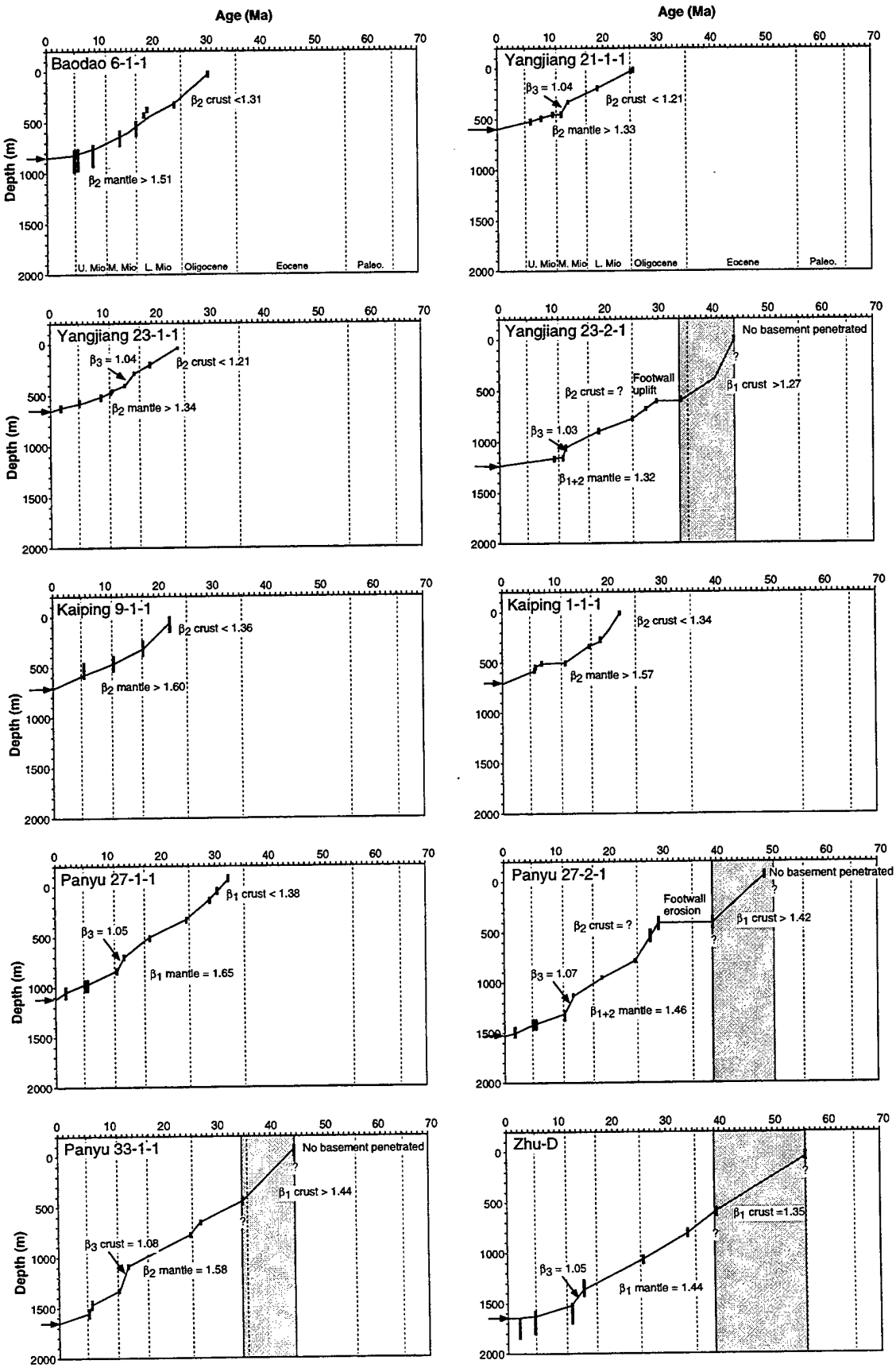

Figure 11. Example of one dimensional backstripping of drilled stratigraphies from the South China Shelf following the procedure of *Sclater and Christie* [1980]. Shaded region shows synrift sedimentation which is not sampled at all sites due to their location on the crests of uplifted footwall blocks. Rifting is of clear Eocene-Oligocene age and seems to have been completed by ~32 Ma, Early Miocene. β1, β2 and β3 are the total extension factors estimated for the three extensional events interpreted from changes in the rates of tectonic subsidence.

break-up, constraining water depths to no more than 200 m. With such high resolution data, the uncertainties introduced from this source are minor, allowing the restored level of the basement to be accurately pin-pointed at any given time. Figure 11 shows ten examples of backstripped wells from South China Sea revealing that the uncertainties are relatively small compared to the total subsidence. This allows detailed comparison of reconstructed basement subsidence with pure shear models [e.g., *McKenzie*, 1978; *Royden and Keen*, 1980], that permit the degree of extension to be estimated. The estimate only applies to the column of lithosphere under the drill site.

By quantifying the amount of syn-rift versus postrift subsidence that has affected the basement ,we can estimate the degree of whole crustal extension compared to mantle extension, since the latter is the only control on the rate of postrift subsidence, while the syn-rift subsidence represents the resultant effect of subsidence due to crustal extension and uplift due to mantle thinning (Fig. 12). A general pattern emerges of higher extension in the central region of the South China Shelf, where the basement deepens within the Pearl River Mouth Basin. The crust appears to extend by at least 55% ($\beta = 1.55$). This basin is then separated from the passive margin proper by a basement high under which extension is <28%. A general trend of crustal extension being less than mantle extension is noted.

4.0 Seismic Velocity Structure

The vertical velocity profile at each of the control points can be compared with the existing estimates of velocity structure based on the expanded spread profiling (ESP) work of *Nissen et al.* [1995b]. Figure 13 shows the vertical variations in compressional wave velocity at each of the ESP stations together with that derived from the closest control point on the multichannel lines. Although the two curves rarely lie right on top of one another, several (e.g., ESP 9 and ESP 16) show excellent agreement throughout the depth section. In most other examples, there is some discrepancy in the deeper parts of the section, where the resolution of the multichannel reflection data is poor, but good agreement in the top 1–2 km. Even in the deeper parts of the section, rapid increases in seismic velocity can be recognized at similar depths in both methods, even if the magnitude of the increase is different in each. In general the ESP velocity profiles tend to give more step-like profiles while the multichannel profiles tend to smooth gradients.

Figure 14 shows the lateral variations in depth to the base of the 1500 m/s velocity interval, i.e., the seabed. This surface is clearly the easiest to cross check because this represents the seafloor, which is well mapped by echo-sounding and is widely published. Comparison of this map with the bathymetry shows an excellent agreement.

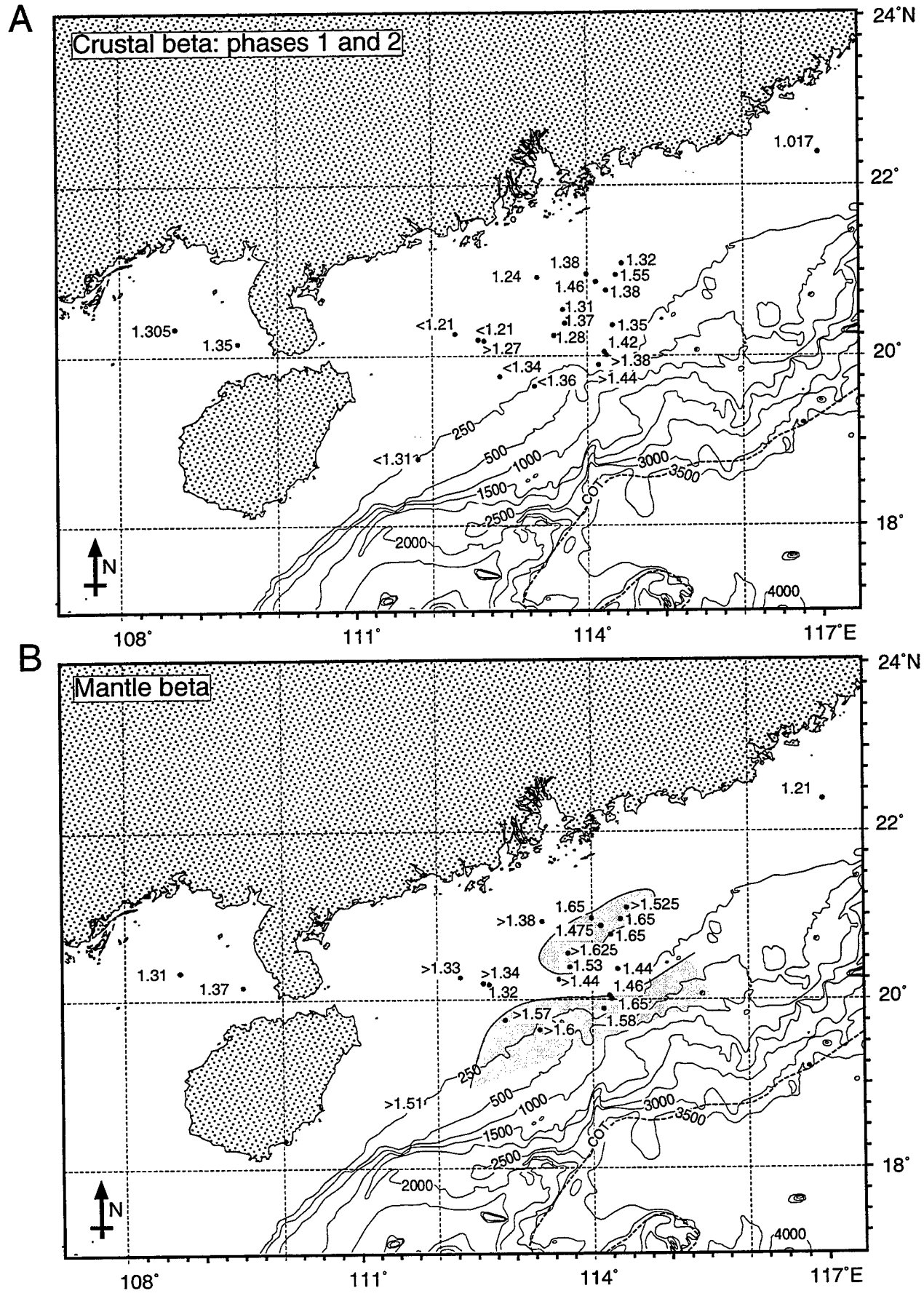

Figure 12. Maps showing variation in crustal (A) and mantle (B) extension over the South China Shelf as derived from the modeling of backstripped well logs. Note higher extension in the central Pearl River Mouth basin compared to the outer high, as well as higher mantle extension compared to crustal extension.

A series of maps are provided in which the depth to different velocity intervals are shown. The velocity intervals chosen are the same as those used by Hayes in his previous study for the Naval Oceanographic Office and reflect naturally occurring divisions in the velocity structure of the South China shelf, revealed by the ESP and now MCS analysis. The contours are chosen at 1500 m/s, 1800 m/s, 2100 m/s, 2400 m/s, 2800 m/s, 3100 m/s, 3400 m/s, 4800 m/s, 6600 m/s and 7200 m/s. For comparison we show the depth contour using just the new data presented in this report, as well as the contour derived from combining the data of Dennis Hayes with the new data. It may be seen that, as suggested from the direct comparison of his ESP data, there is a good agreement between the two sets.

It is noteworthy that while the slower shallower velocity contours tended to be smooth surface, as one might expect, this pattern became more disrupted with increasing velocity. This is because the higher velocity layers correspond to the more compacted sediments and crystalline basement (estimated at > 4800 m/s), which were involved to a greater degree in the faulting that formed the South China Sea. For these layers the assumption of a simple blanketing sedimentation pattern is clearly not feasible, so that rapid lateral breaks in the velocity might be anticipated, especially across faults. For example, there is a marked shallowing of the high velocity layers in the eastern part of the shelf, which correlates with a shallowing of the basement interpreted from the reflection profiles (see Profile 1716 in Figure 7). This structural high separates the Pearl River Mouth Basin from the South China Slope. In addition, the poorer quality of the MCS stacking data at significant depths adds noise and uncertainty into the plots that may not correspond on the fine scale with the actual sub-seafloor structure. When compiling the data we have attempted to reduce extraneous noise by filtering out data implying large reductions in seismic velocity with increasing depth. Although the stacking velocities do frequently imply a velocity inversion, and this is clearly feasible in theory, in practise most of these were the result of poor data quality at depth. Thus we removed all data indicating velocity drops of > 50 m/s, especially within the basement units (V_{dix} > 4800 m/s) This filtering process is justified in order to make the data more compatible with that of Hayes, and to be consistent with what is know of the margin structure from drilling data.

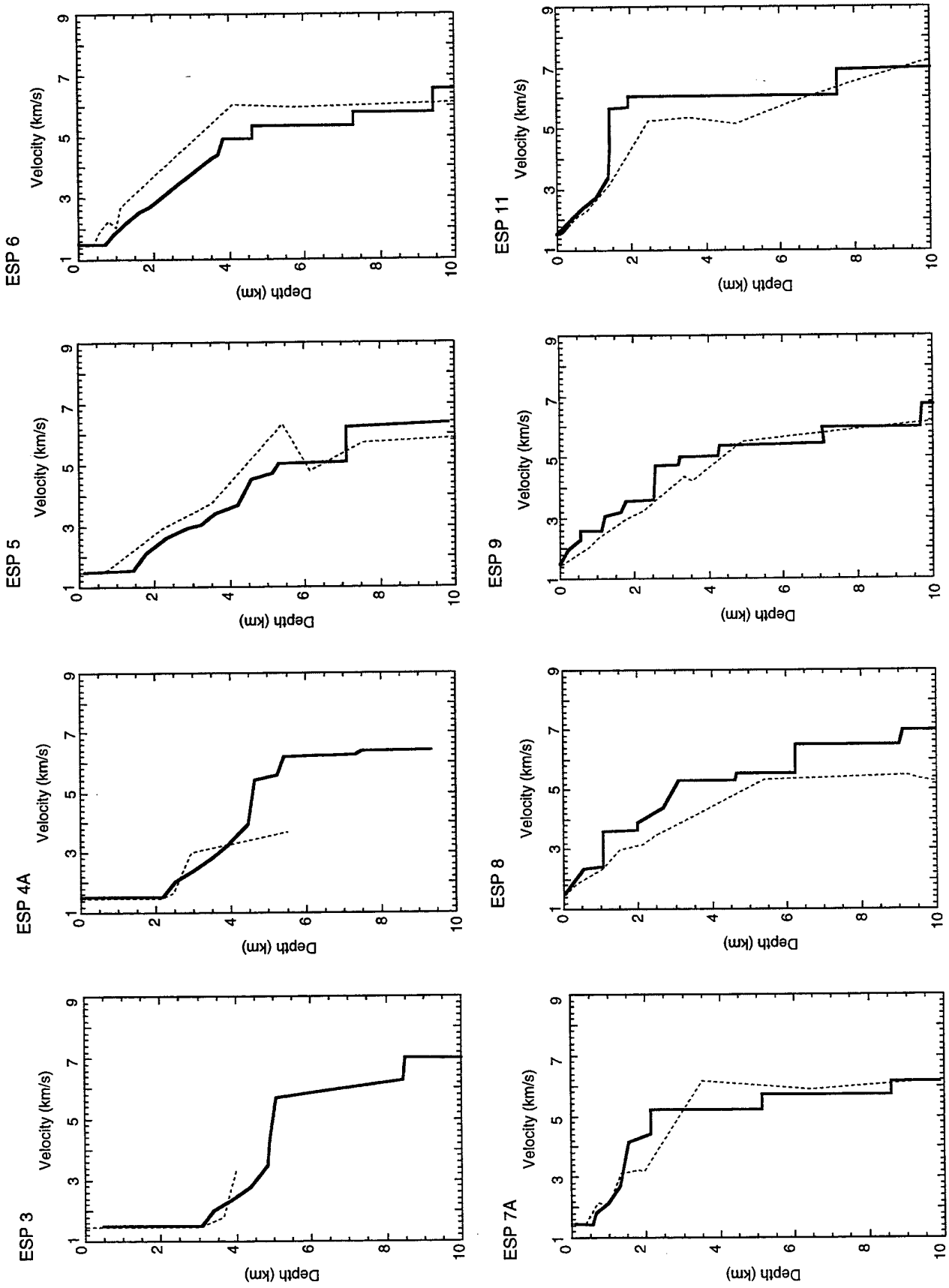

Figure 13. Velocity-depth plots from the South China Shelf, showing the predictions derived from EPS surveys [*Nissen et al.*, 1995b; solid lines] and those from the stacking velocities of the multichannel reflection surveys (dashed lines).

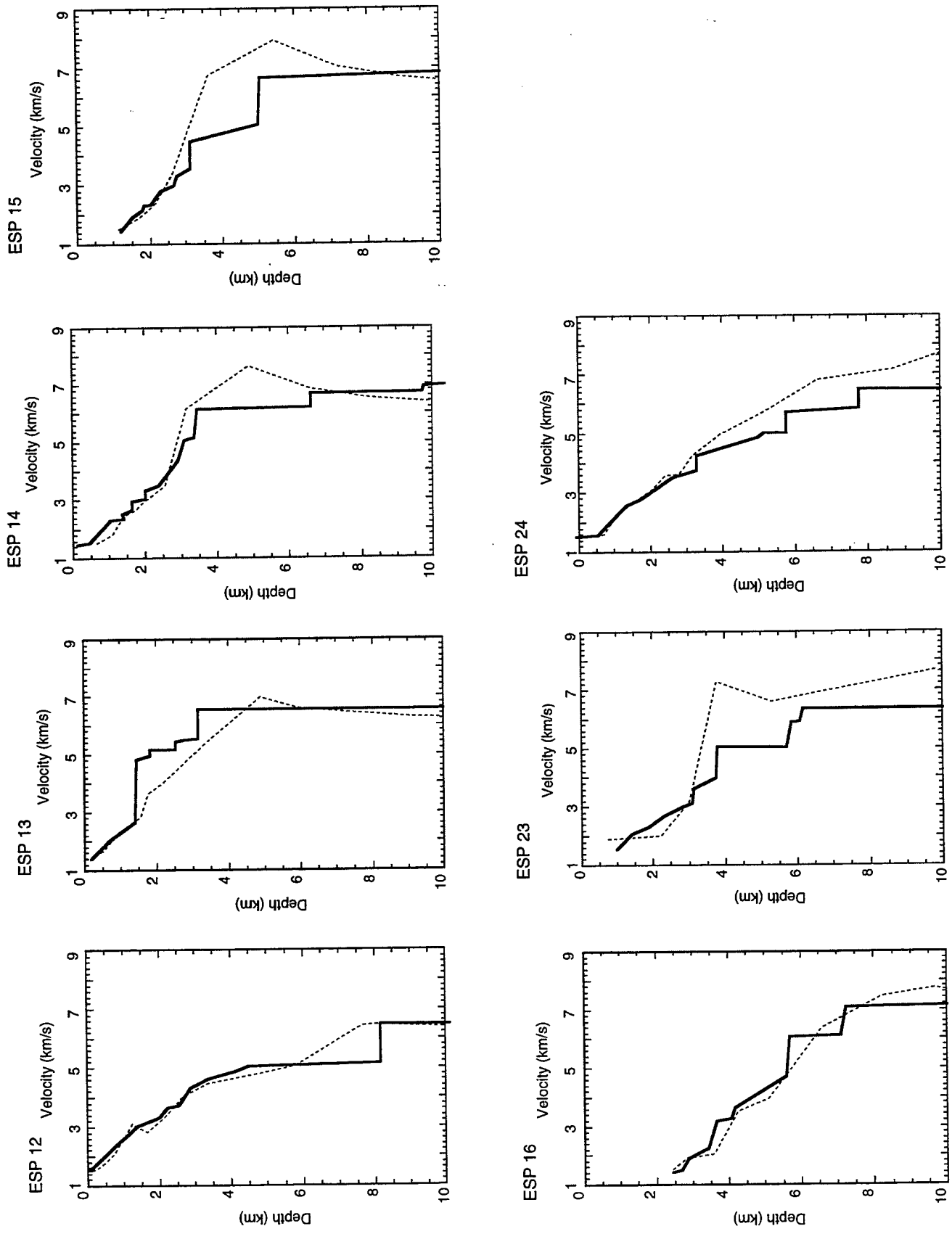
ESP 15
ESP 14
ESP 24
ESP 13
ESP 23
ESP 12
ESP 16
Velocity (km/s)
Depth (km)

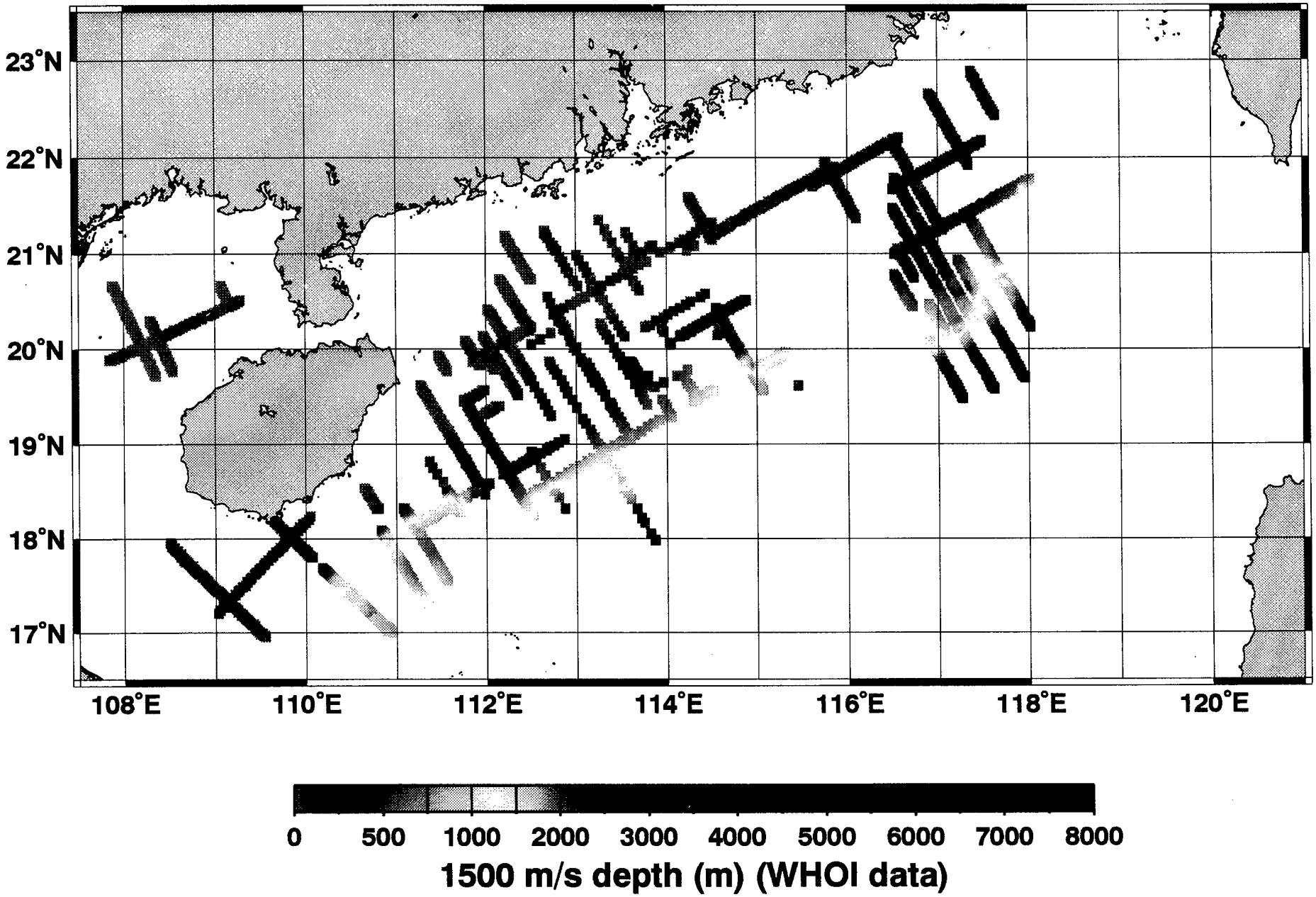
23°N
22°N
21°N
20°N
19°N
18°N
17°N
108°E
110°E
112°E
114°E
116°E
118°E
120°E
0
500
1000
2000
3000
4000
5000
6000
7000
8000
1500 m/s depth (m) (WHOI data)

Figure 14

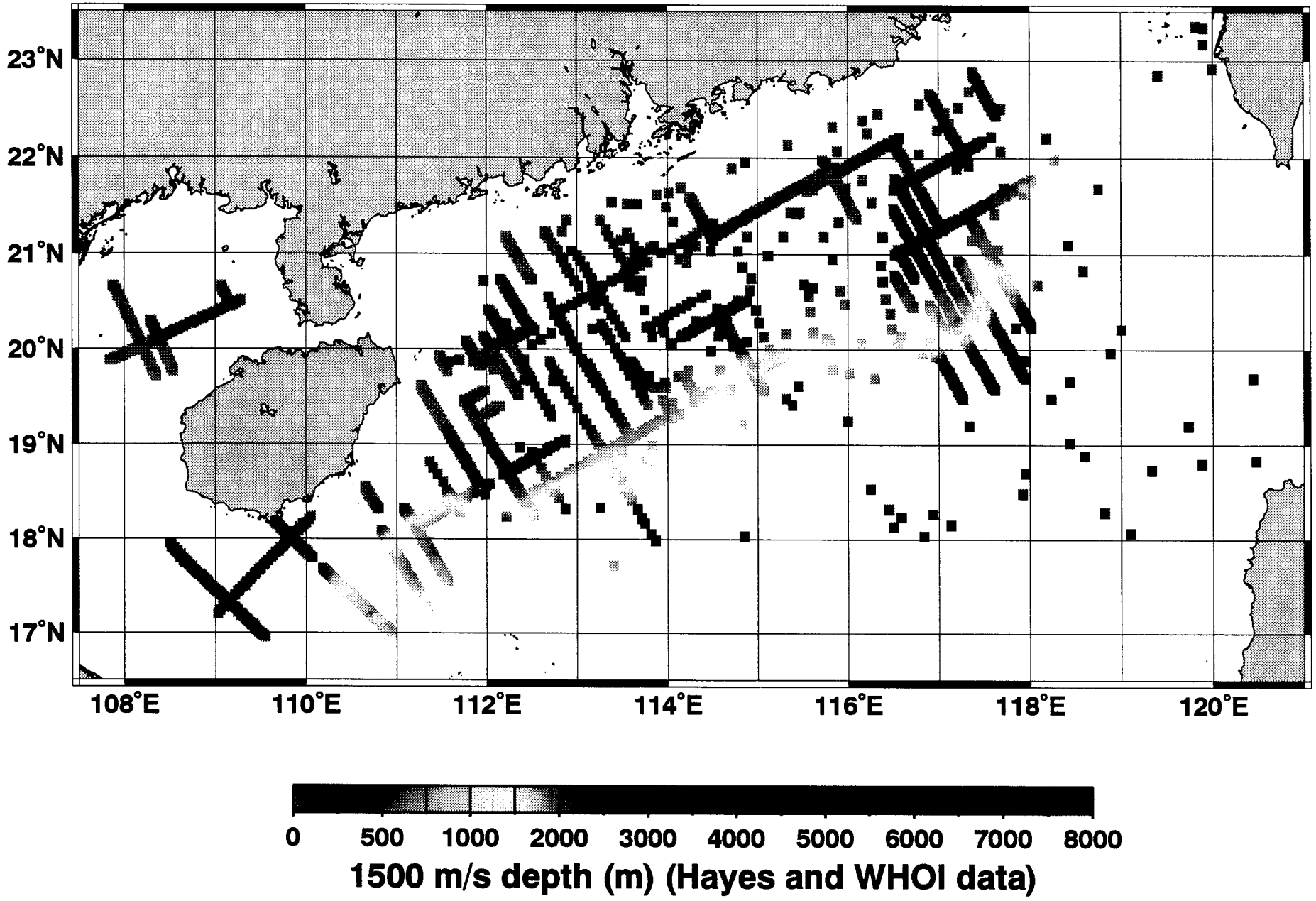
23°N
22°N
21°N
20°N
19°N
18°N
17°N
108°E
110°E
112°E
114°E
116°E
118°E
120°E
0
500
1000
2000
3000
4000
5000
6000
7000
8000
1500 m/s depth (m) (Hayes and WHOI data)

Figure 15

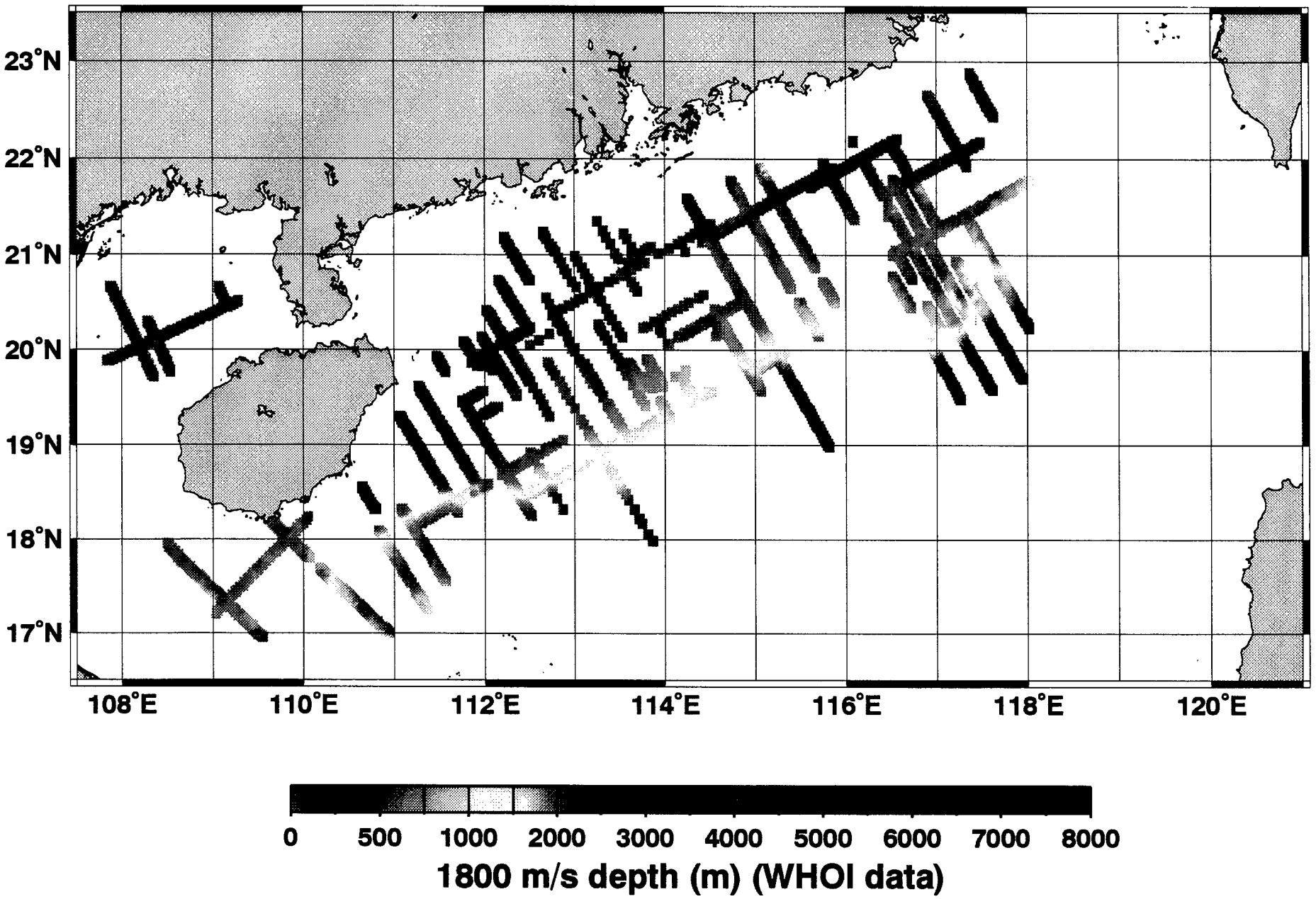
23°N
22°N
21°N
20°N
19°N
18°N
17°N
108°E
110°E
112°E
114°E
116°E
118°E
120°E
0
500
1000
2000
3000
4000
5000
6000
7000
8000
1800 m/s depth (m) (WHOI data)

Figure 16

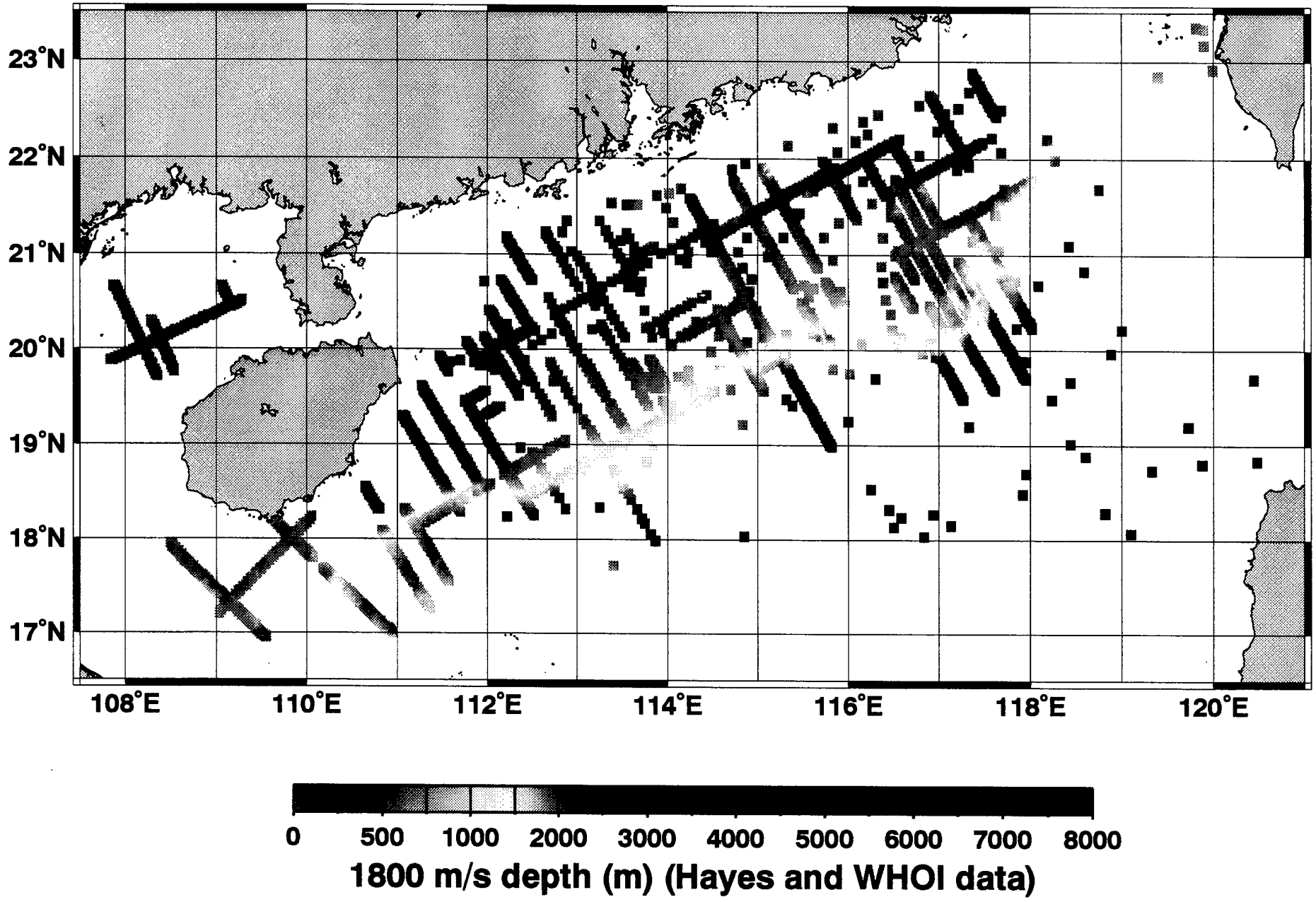
23°N
22°N
21°N
20°N
19°N
18°N
17°N
108°E
110°E
112°E
114°E
116°E
118°E
120°E
0
500
1000
2000
3000
4000
5000
6000
7000
8000
1800 m/s depth (m) (Hayes and WHOI data)

Figure 17

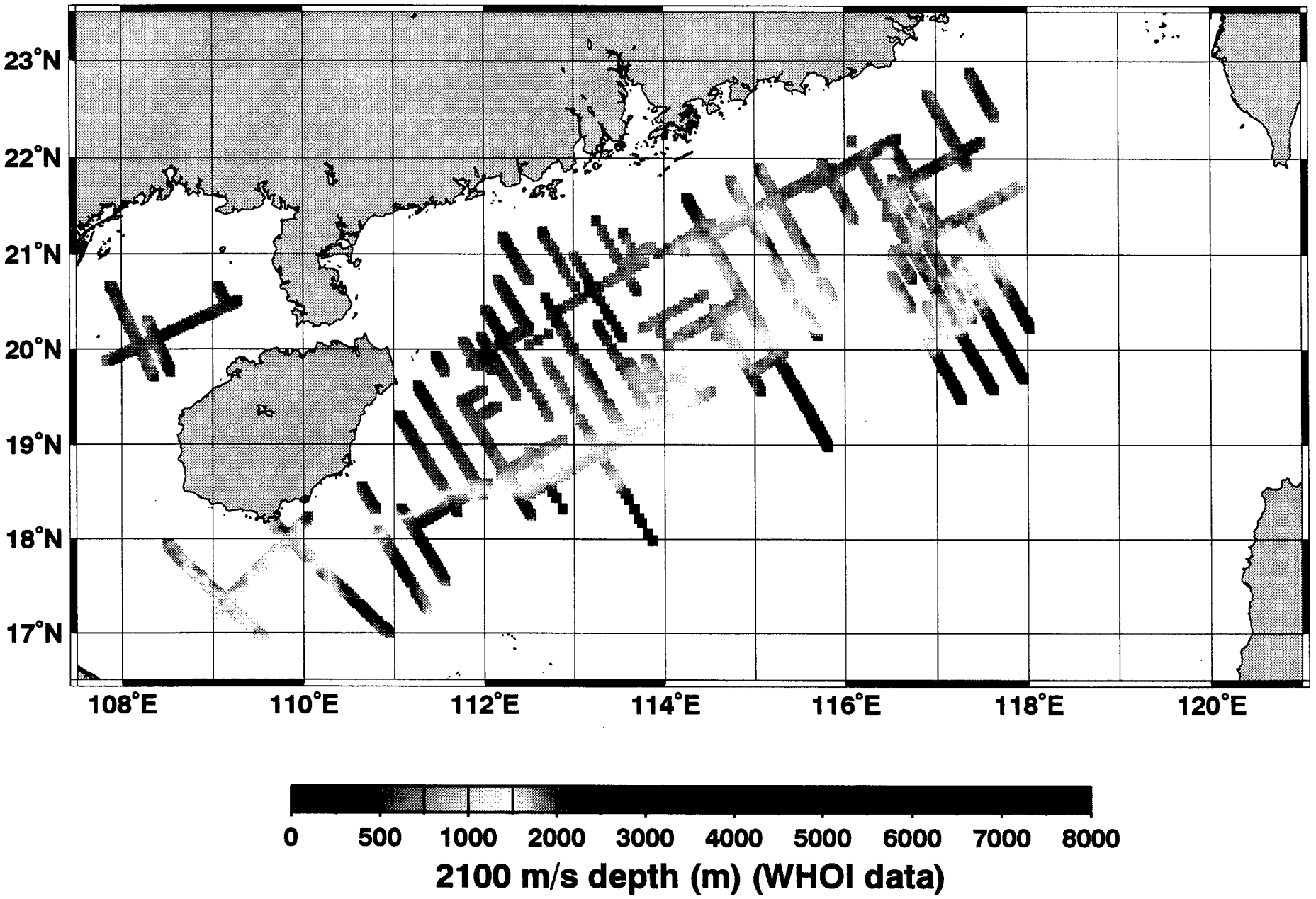
23°N
22°N
21°N
20°N
19°N
18°N
17°N
108°E
110°E
112°E
114°E
116°E
118°E
120°E
0
500
1000
2000
3000
4000
5000
6000
7000
8000
2100 m/s depth (m) (WHOI data)

Figure 18

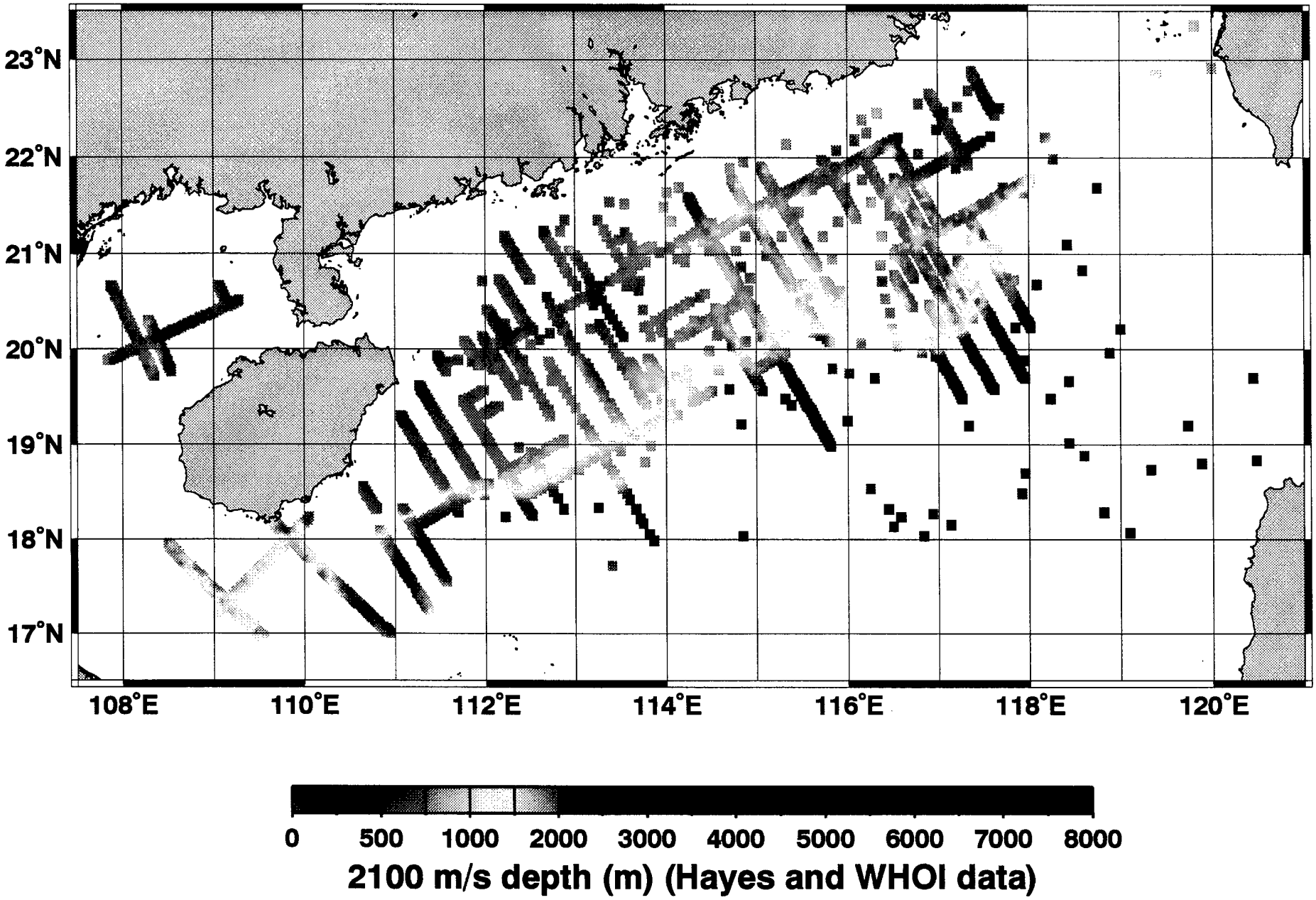
23°N
22°N
21°N
20°N
19°N
18°N
17°N
108°E
110°E
112°E
114°E
116°E
118°E
120°E
0
500
1000
2000
3000
4000
5000
6000
7000
8000
2100 m/s depth (m) (Hayes and WHOI data)

Figure 19

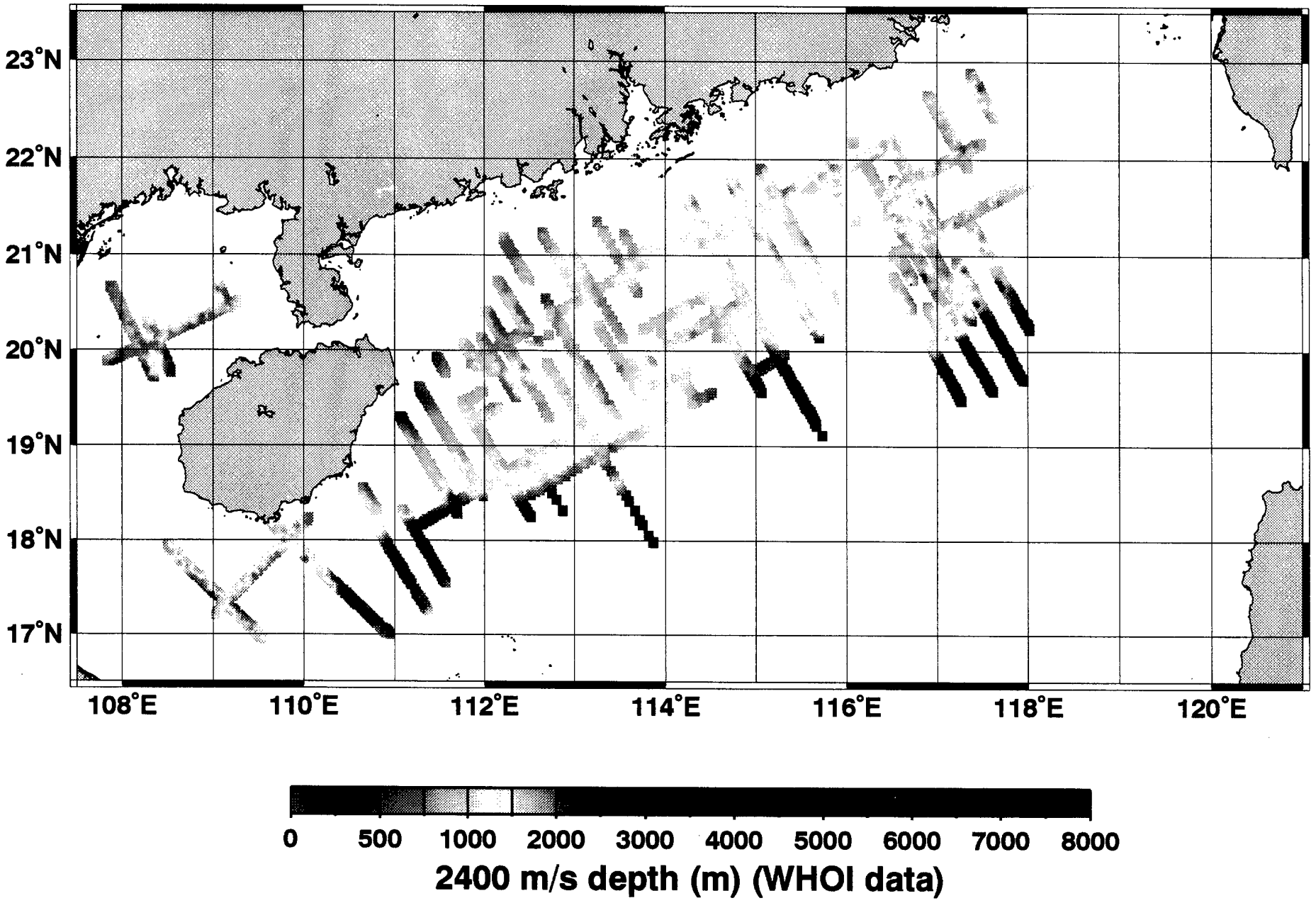
23°N
22°N
21°N
20°N
19°N
18°N
17°N
108°E
110°E
112°E
114°E
116°E
118°E
120°E
0
500
1000
2000
3000
4000
5000
6000
7000
8000
2400 m/s depth (m) (WHOI data)

Figure 20

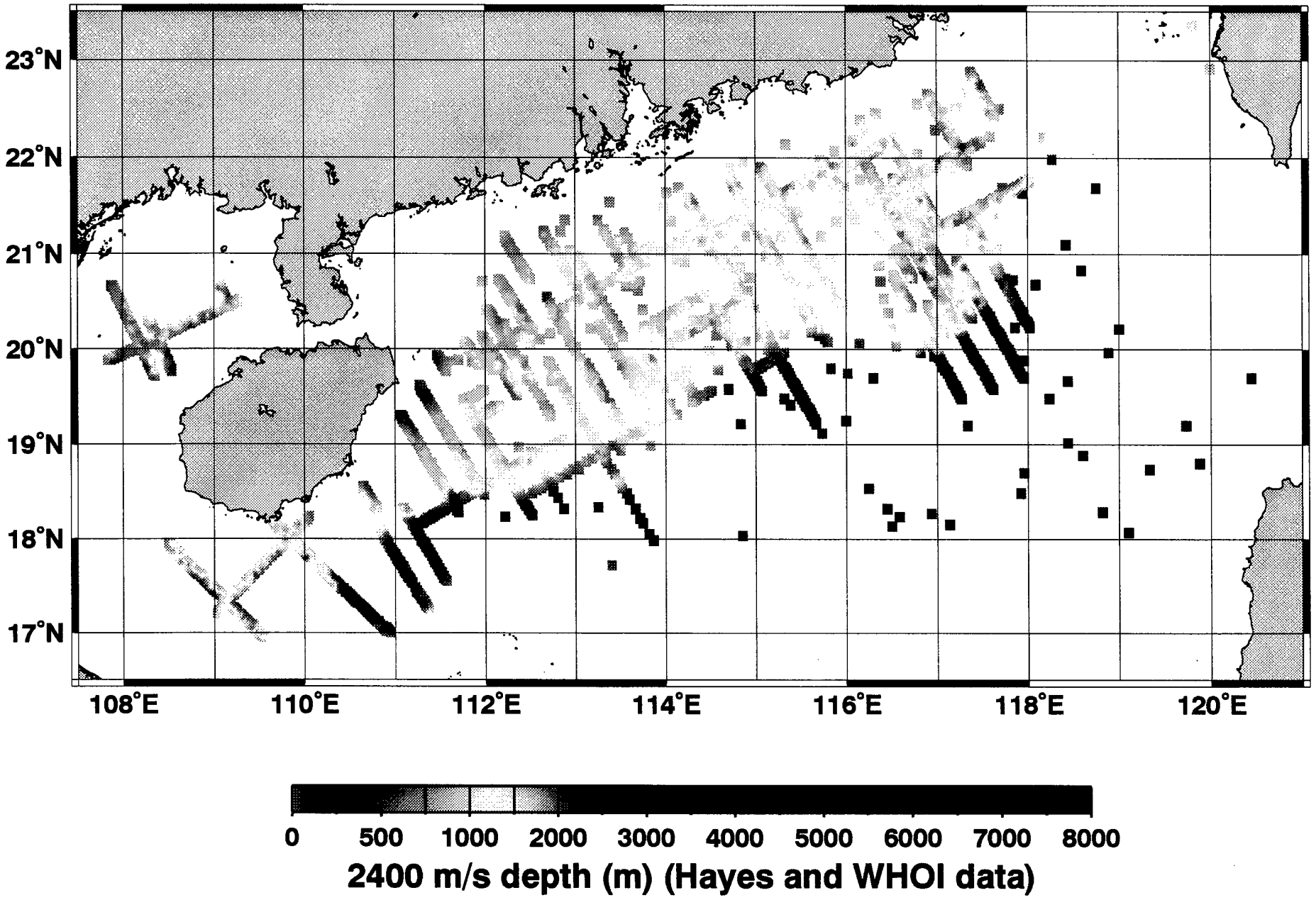
23°N
22°N
21°N
20°N
19°N
18°N
17°N
108°E
110°E
112°E
114°E
116°E
118°E
120°E
0
500
1000
2000
3000
4000
5000
6000
7000
8000
2400 m/s depth (m) (Hayes and WHOI data)

Figure 21

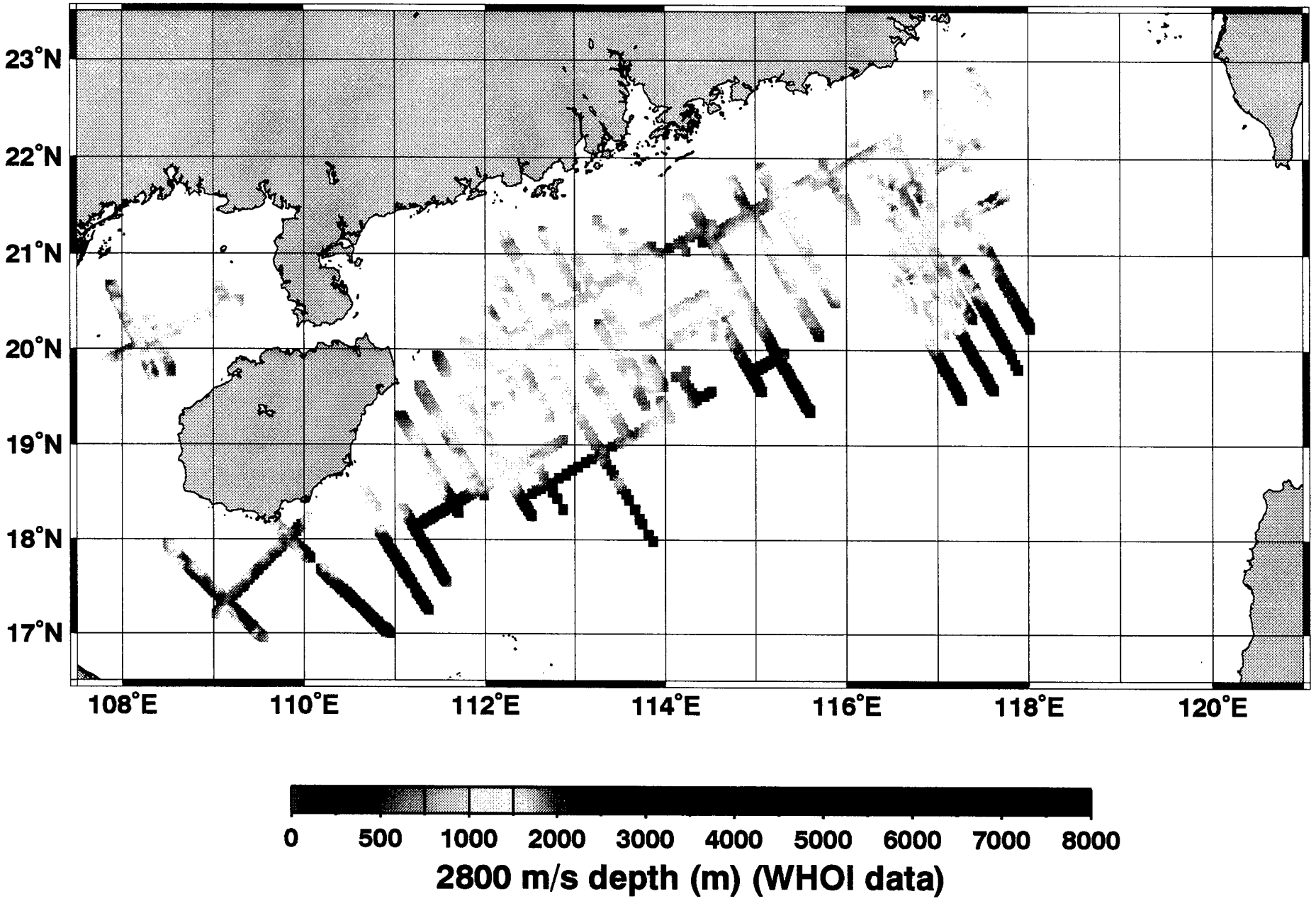
23°N
22°N
21°N
20°N
19°N
18°N
17°N
108°E
110°E
112°E
114°E
116°E
118°E
120°E
0
500
1000
2000
3000
4000
5000
6000
7000
8000
2800 m/s depth (m) (WHOI data)

Figure 22

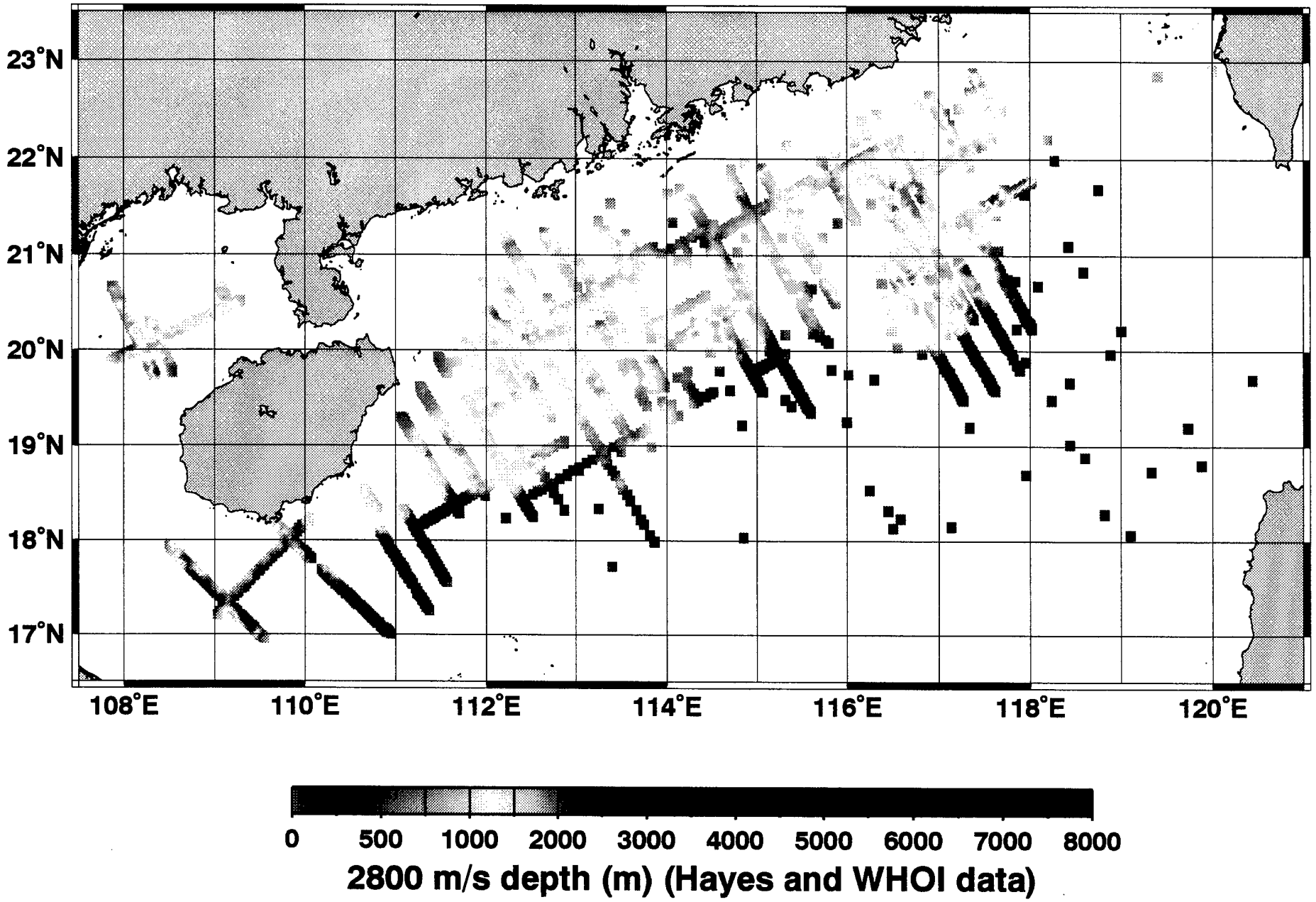
23°N
22°N
21°N
20°N
19°N
18°N
17°N
108°E
110°E
112°E
114°E
116°E
118°E
120°E
0
500
1000
2000
3000
4000
5000
6000
7000
8000
2800 m/s depth (m) (Hayes and WHOI data)

Figure 23

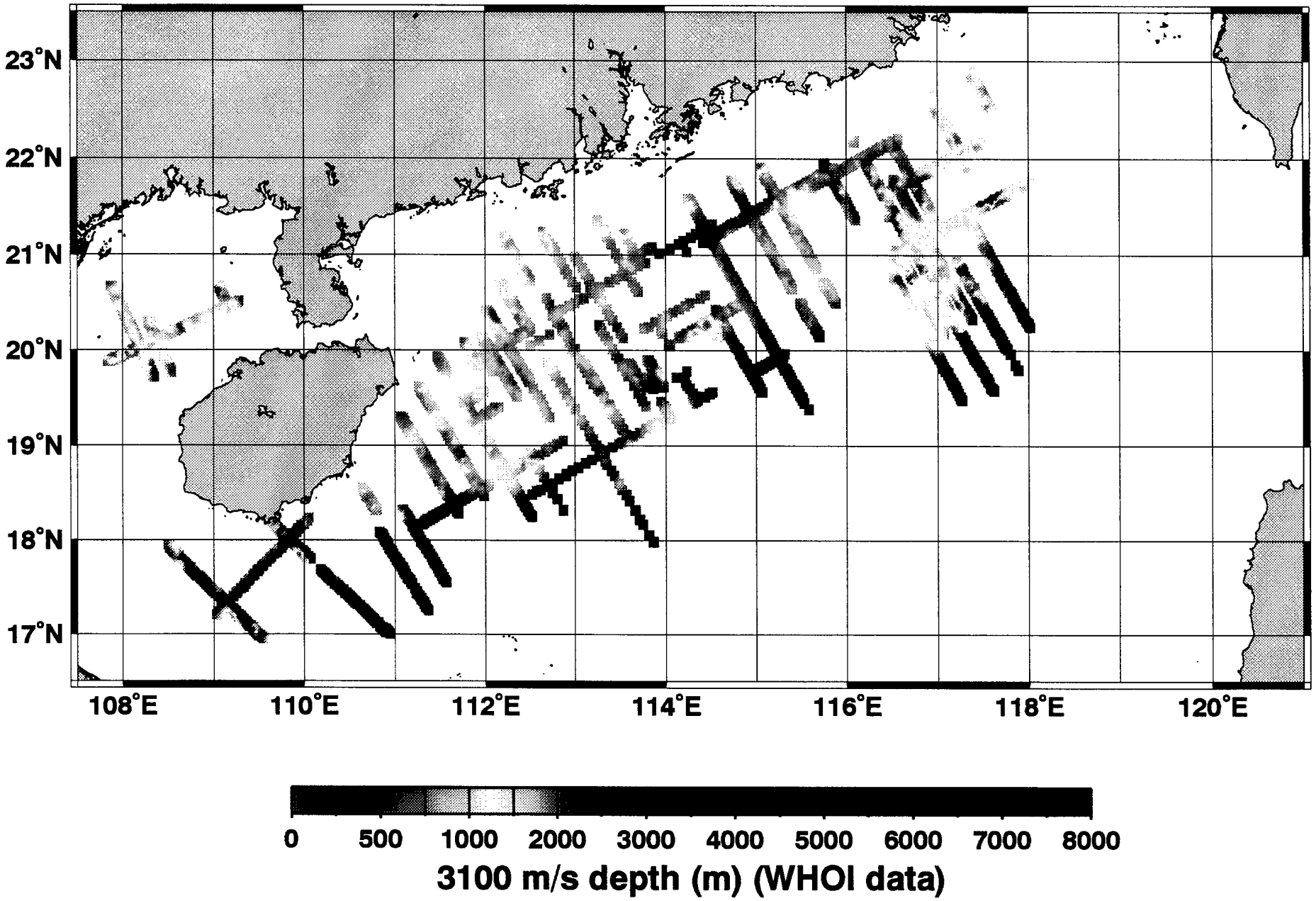
23°N
22°N
21°N
20°N
19°N
18°N
17°N
108°E
110°E
112°E
114°E
116°E
118°E
120°E
0
500
1000
2000
3000
4000
5000
6000
7000
8000
3100 m/s depth (m) (WHOI data)

Figure 24

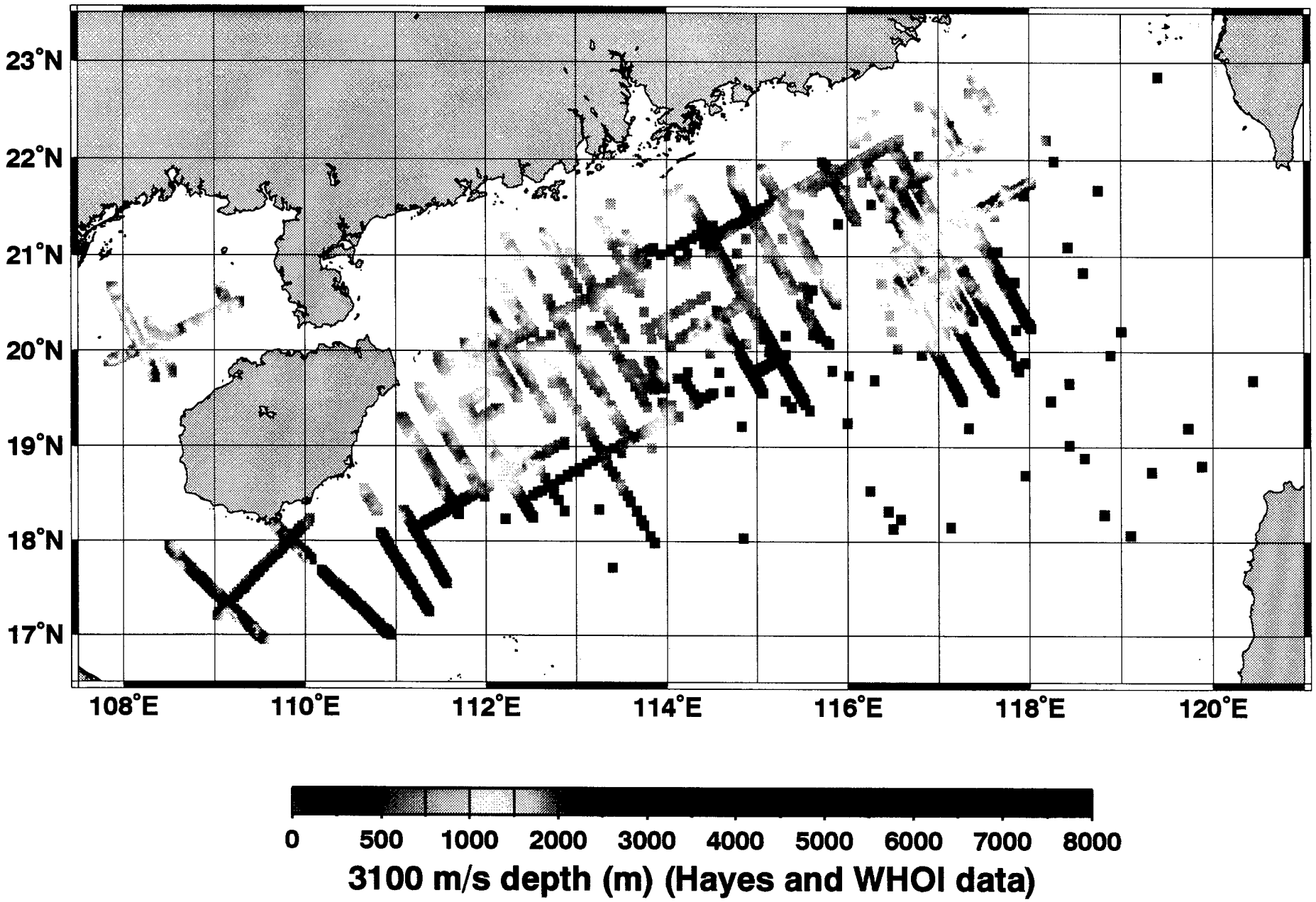
23°N
22°N
21°N
20°N
19°N
18°N
17°N
108°E
110°E
112°E
114°E
116°E
118°E
120°E
0
500
1000
2000
3000
4000
5000
6000
7000
8000
3100 m/s depth (m) (Hayes and WHOI data)

Figure 25

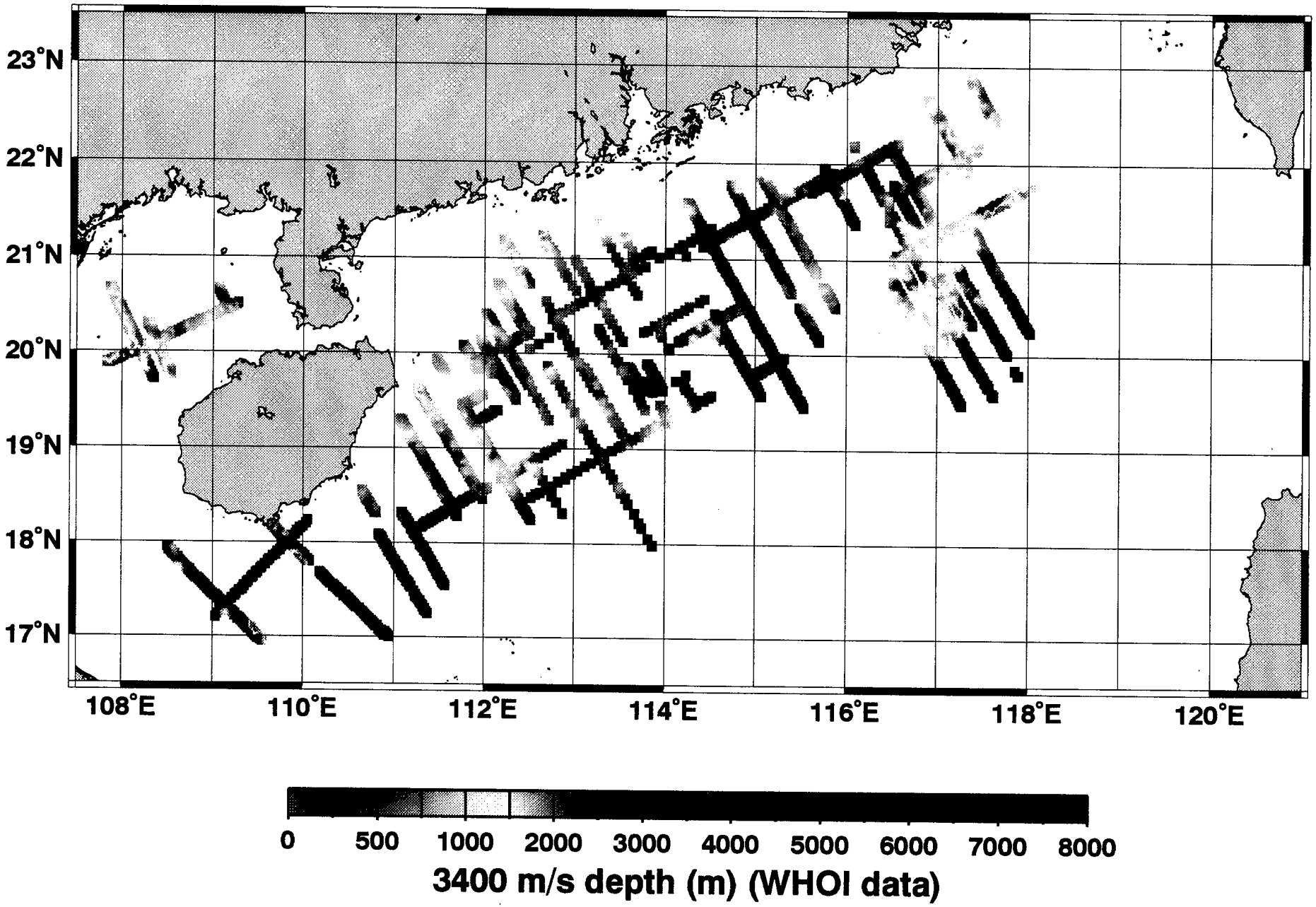
23°N
22°N
21°N
20°N
19°N
18°N
17°N
108°E
110°E
112°E
114°E
116°E
118°E
120°E
0
500
1000
2000
3000
4000
5000
6000
7000
8000
3400 m/s depth (m) (WHOI data)

Figure 26

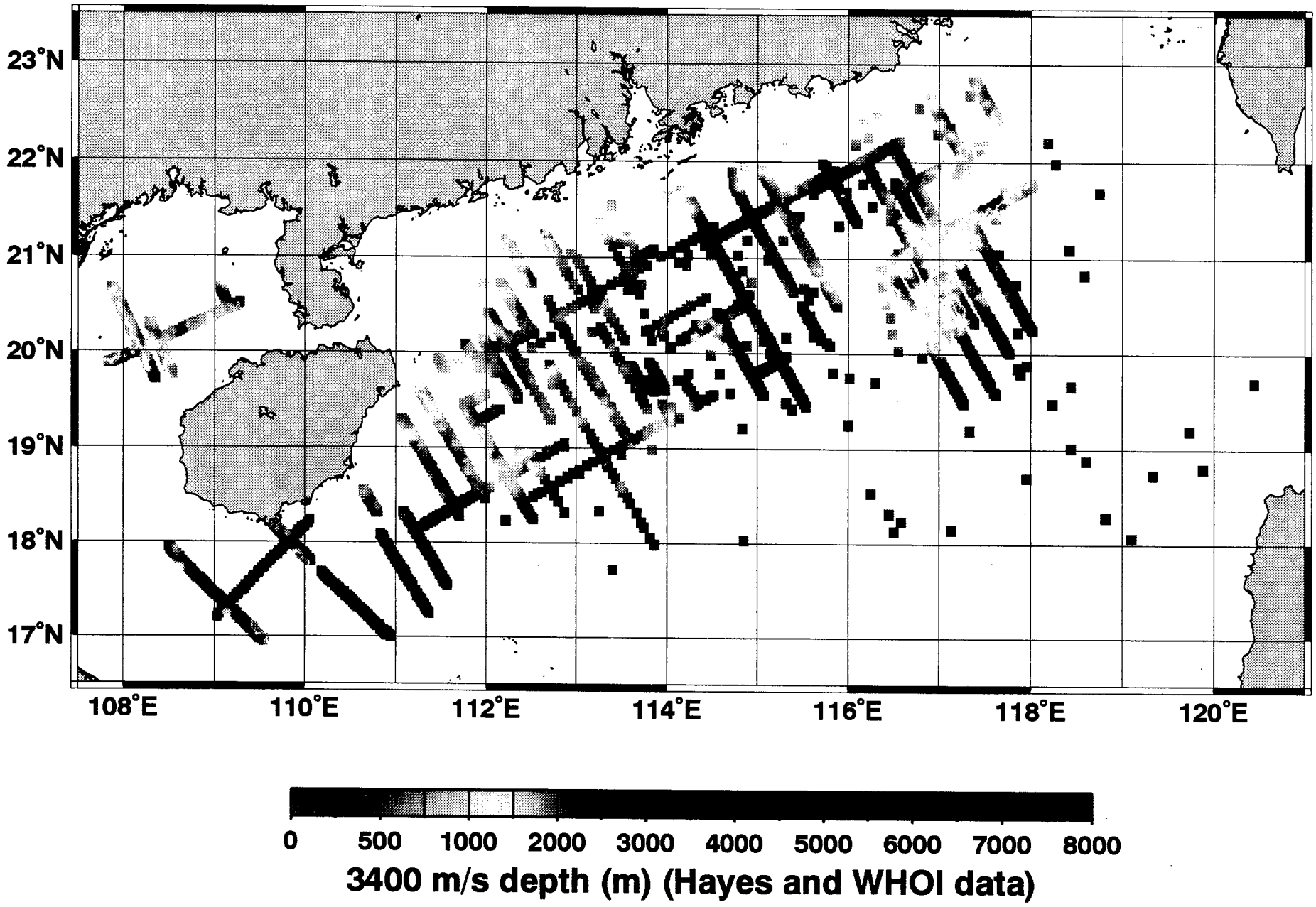
23°N
22°N
21°N
20°N
19°N
18°N
17°N
108°E
110°E
112°E
114°E
116°E
118°E
120°E
0
500
1000
2000
3000
4000
5000
6000
7000
8000
3400 m/s depth (m) (Hayes and WHOI data)

Figure 27

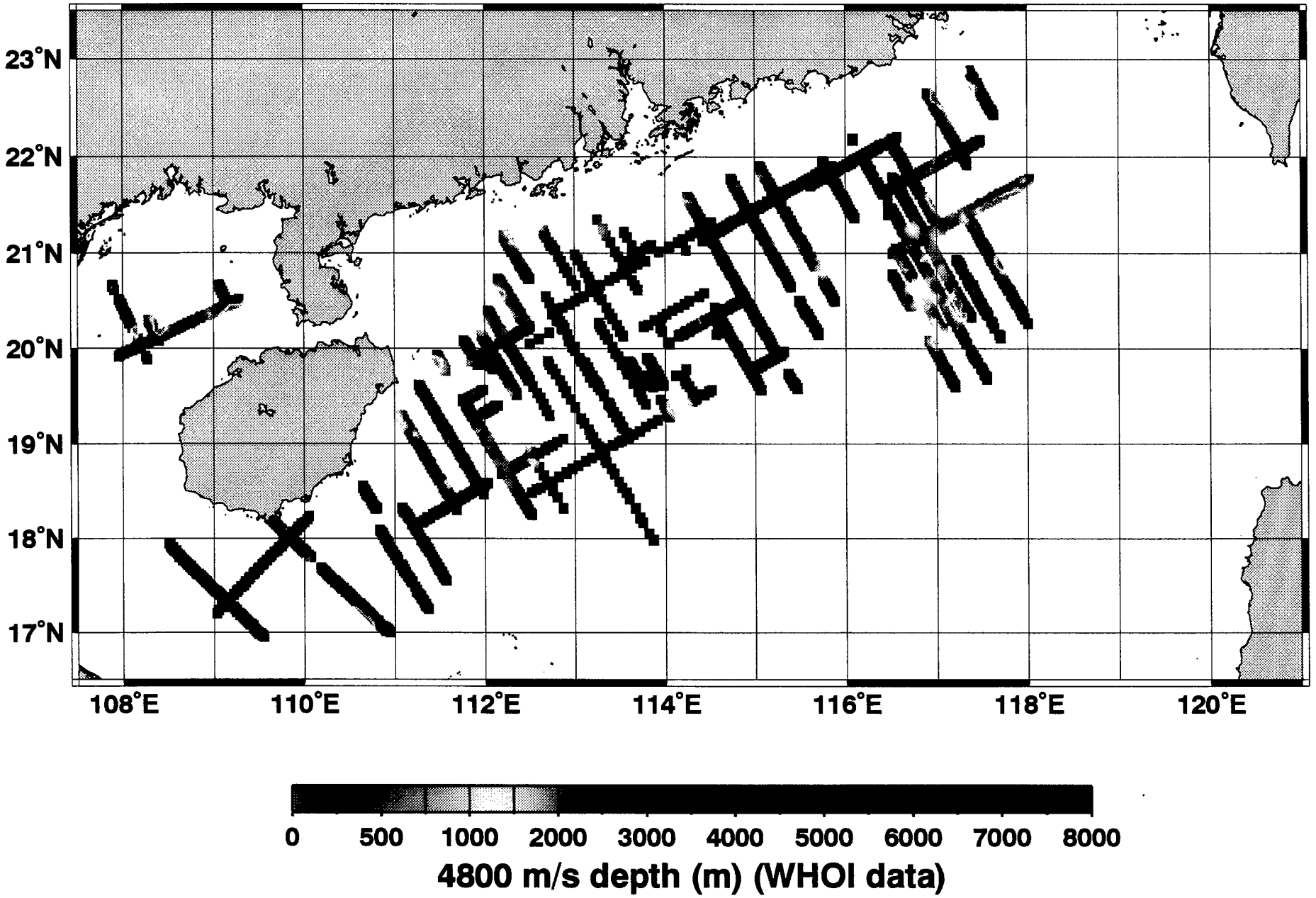
23°N
22°N
21°N
20°N
19°N
18°N
17°N
108°E
110°E
112°E
114°E
116°E
118°E
120°E
0
500
1000
2000
3000
4000
5000
6000
7000
8000
4800 m/s depth (m) (WHOI data)

Figure 28

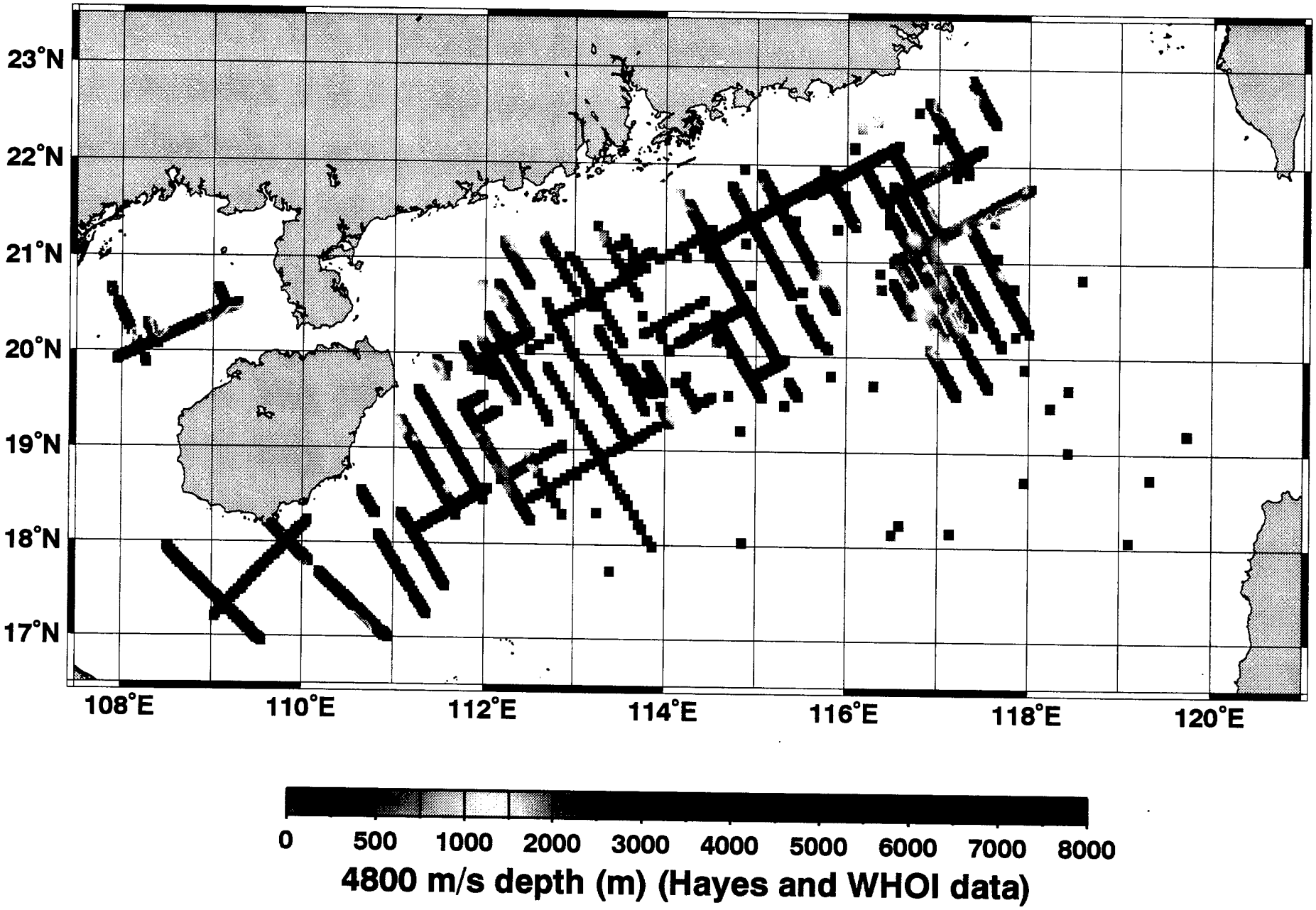
23°N
22°N
21°N
20°N
19°N
18°N
17°N
108°E
110°E
112°E
114°E
116°E
118°E
120°E
0
500
1000
2000
3000
4000
5000
6000
7000
8000
4800 m/s depth (m) (Hayes and WHOI data)

Figure 29

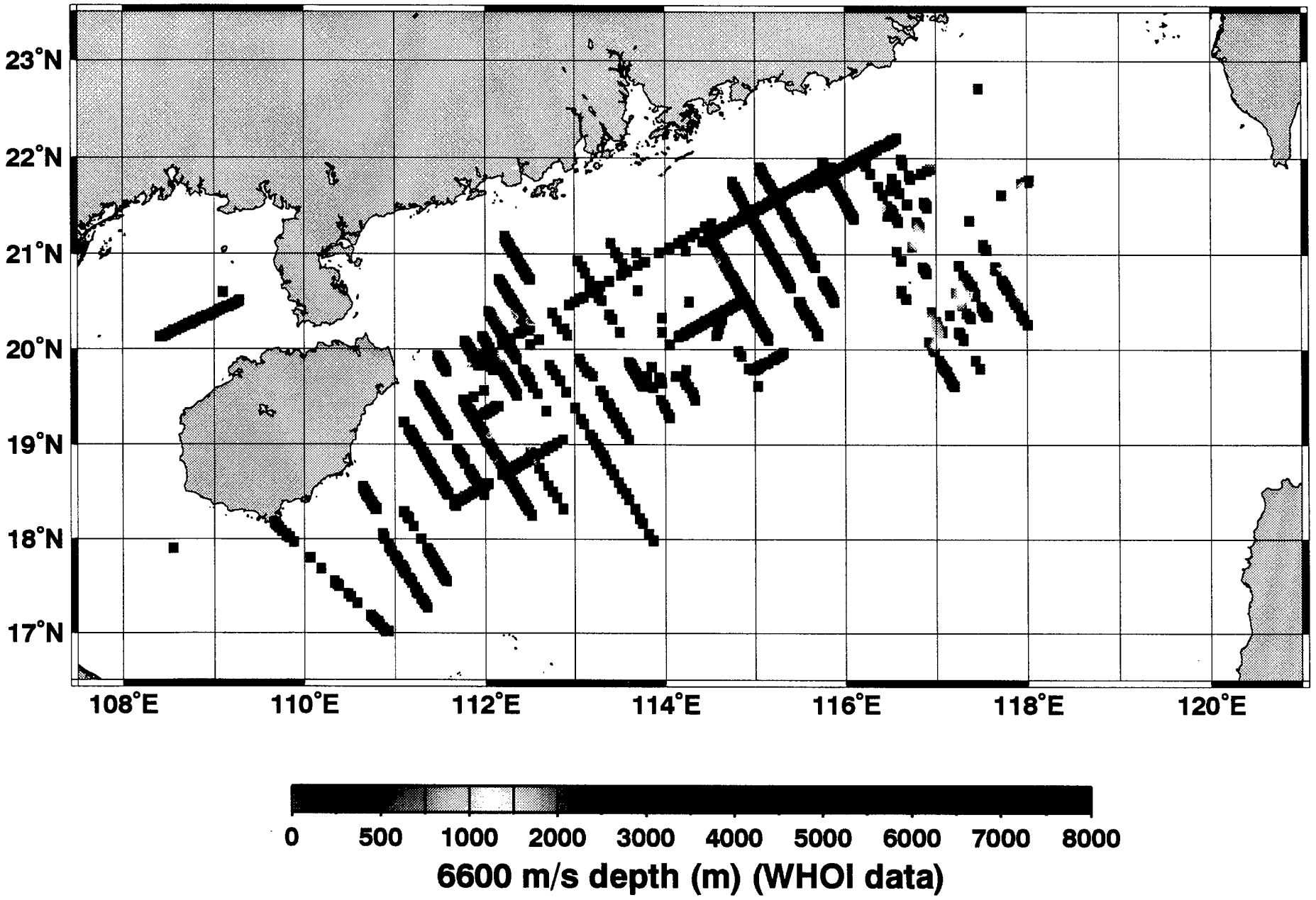
23°N
22°N
21°N
20°N
19°N
18°N
17°N
108°E
110°E
112°E
114°E
116°E
118°E
120°E
0
500
1000
2000
3000
4000
5000
6000
7000
8000
6600 m/s depth (m) (WHOI data)

Figure 30

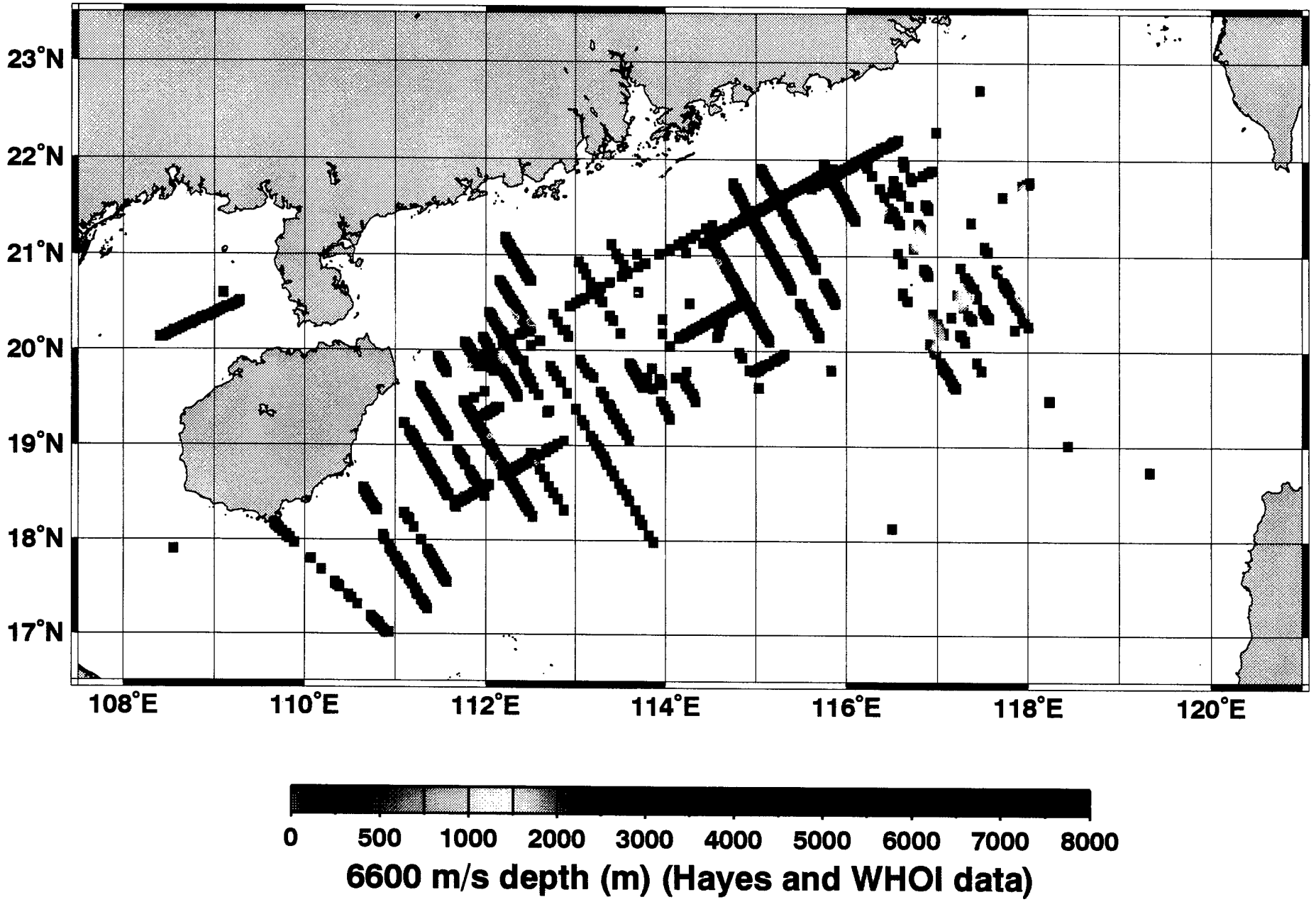
23°N
22°N
21°N
20°N
19°N
18°N
17°N
108°E
110°E
112°E
114°E
116°E
118°E
120°E
0
500
1000
2000
3000
4000
5000
6000
7000
8000
6600 m/s depth (m) (Hayes and WHOI data)

Figure 31

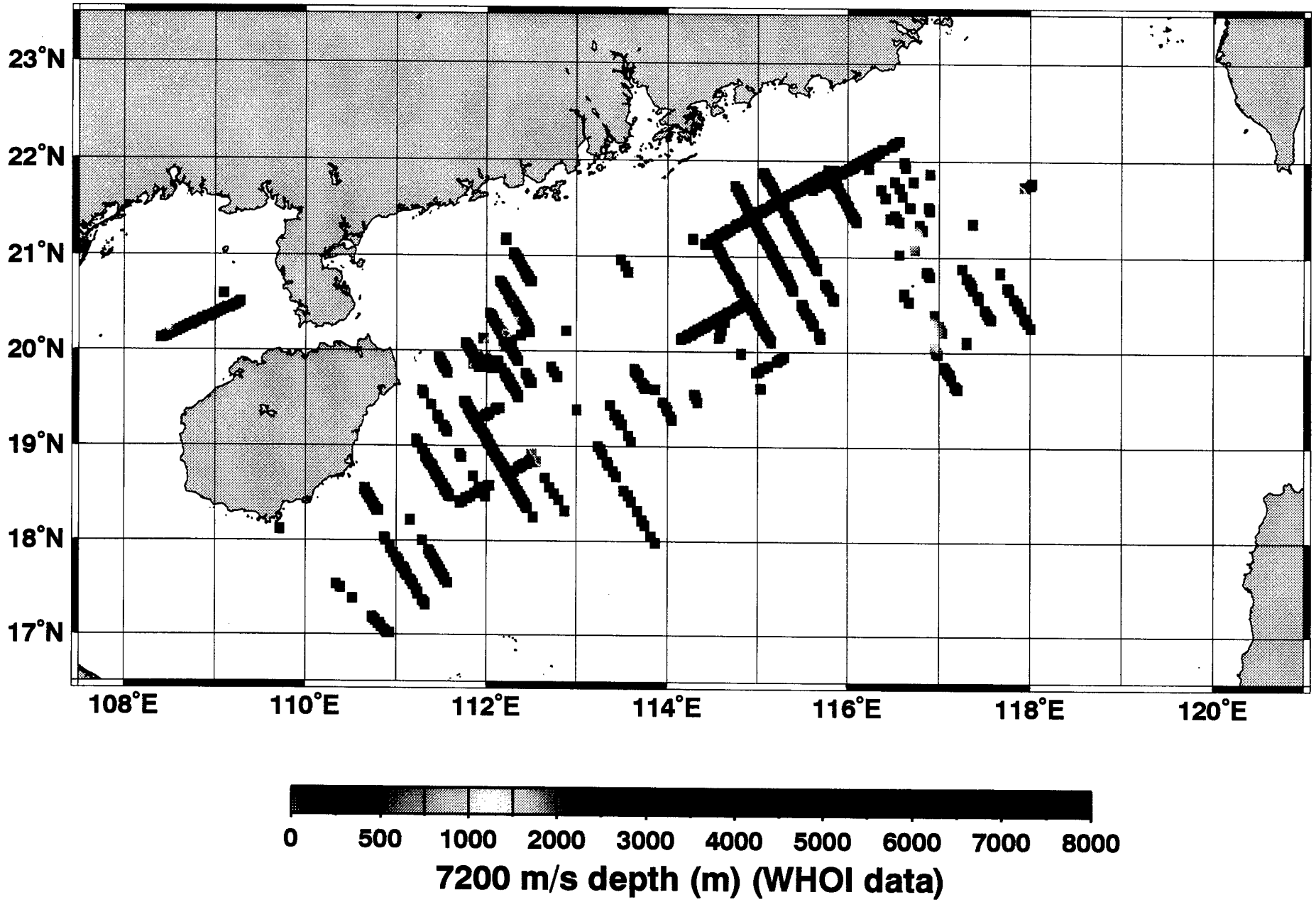
23°N
22°N
21°N
20°N
19°N
18°N
17°N
108°E
110°E
112°E
114°E
116°E
118°E
120°E
0
500
1000
2000
3000
4000
5000
6000
7000
8000
7200 m/s depth (m) (WHOI data)

Figure 32

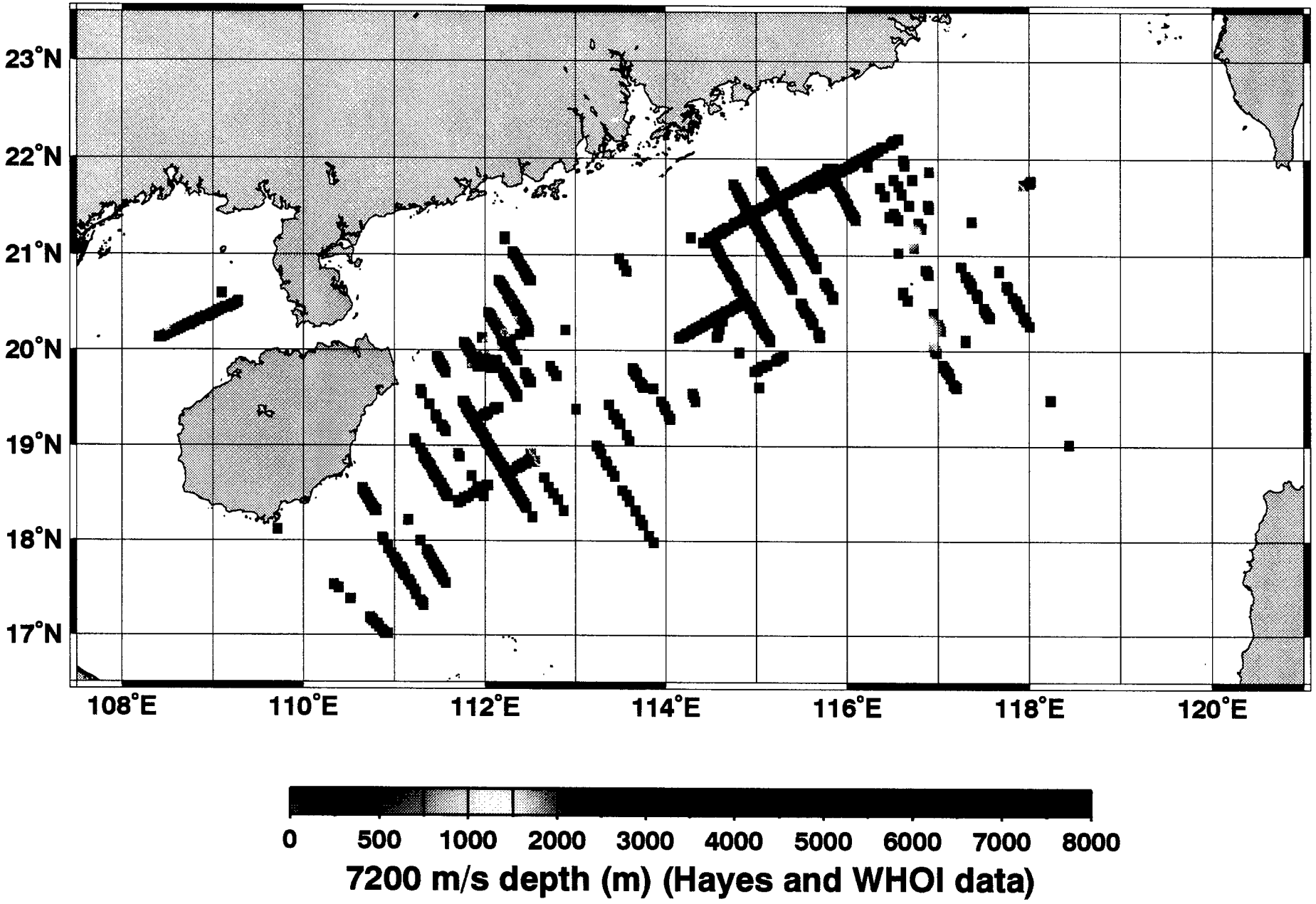
23°N
22°N
21°N
20°N
19°N
18°N
17°N
108°E
110°E
112°E
114°E
116°E
118°E
120°E
0
500
1000
2000
3000
4000
5000
6000
7000
8000
7200 m/s depth (m) (Hayes and WHOI data)

Figure 33